THE UNIVERSITY OF TURKISH AERONAUTICAL ASSOCIATION

INSTITUTE OF SCIENCE AND TECHNOLOGY

NUMERICAL AND EXPERIMENTAL PERFORMANCE OF CONCENTRATED SOLAR COLLECTOR WITH DIRECT HEAT EXCHANGE USING NONE-CIRCULATED NANOFLUID

Master Thesis

Waqas Saad AL-KHAZRAJI

Mechanical and Aeronautical Engineering Department

Master Thesis Program

November, 2017

THE UNIVERSITY OF TURKISH AERONAUTICAL ASSOCIATION

INSTITUTE OF SCIENCE AND TECHNOLOGY

NUMERICAL AND EXPERIMENTAL PERFORMANCE OF CONCENTRATED SOLAR COLLECTOR WITH DIRECT HEAT EXCHANGE USING NONE-CIRCULATED NANOFLUID
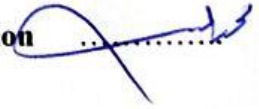
Master Thesis

Waqas Saad AL-KHAZRAJI

1506080018

Mechanical and Aeronautical Engineering Department

Master Thesis Program

Supervisor: Assist. Prof. Dr. Mohamed Salem Elmnefi

Waqas Saad Abdulrazzaq AL-KHAZRAJI, having student number 1506080018 and enrolled in the Master Program at the Institute of Science and Technology at the University of Turkish Aeronautical Association, after meeting all of the required conditions contained in the related regulations, has successfully accomplished, in front of the jury, the presentation of the thesis prepared with the title of: "NUMERICAL AND EXPERIMENTAL PERFORMANCE OF CONCENTRATED SOLAR COLLECTOR WITH DIRECT HEAT EXCHANGE USING NONE-CIRCULATED NANOFLUID".
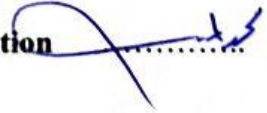
Supervisor : **Assist. Prof. Dr. Mohamed Salem Elmnefi**
    University of Turkish Aeronautical Association

Jury Members : **Assoc. Prof. Dr. Çetin ŞENTÜRK**
    University of Turkish Aeronautical Association

: **Assist. Prof. Dr. Mohamed Salem Elmnefi**
    University of Turkish Aeronautical Association

: **Assist. Prof. Dr. Munir ELFARRA**
    Yildirim Beyazit University- Ankara

Thesis Defense Date: 23.11.2017

THE UNIVERSITY OF TURKISH AERONAUTICAL ASSOCIATION

INSTITUTE OF SCIENCE AND TECHNOLOGY

I hereby declare that all the information in this study I presented as my Master's Thesis, called "Numerical And Experimental Performance of Concentrated Solar Collector with Direct Heat Exchange Using None-Circulated Nanofluid" has been presented in accordance with the academic rules and ethical conduct. I also declare and certify on my honor that I have fully cited and referenced all the sources I made use of in this present study.

Date 23/11/2017

Waqas Saad AL-KHAZRAJI

ACKNOWLEDGEMENTS

TABLE OF CONTENTS

LIST OF TABLES

TABLE OF FIGURE

LIST OF SYMBOLS

$\bar{q}$	Convective heat transfer per unit length [W/m]
$\dot{m}$	Mass flow rate [kg/s]
φ	Volume fraction of Nano-fluid [%]
A_a	Collector's area [m^2]
C_R	Collector's Concentration ratio [dimensionless]
C_p	Specific heat capacity [J/(kg K)]
D_{gi}	Inner diameter of receiver glass tube [mm]
D_{go}	Outer diameter of glass tube [mm]
D_{ci}	Inner diameter of receiver copper tube [mm]
D_{co}	Outer diameter of receiver copper tube [mm]
D_{sp}	Nanoparticles dimeter [nm]
g	Gravitational acceleration [m/s^2]
$\mathcal{F}$	Optical efficiency [dimensionless]
G	Solar radiation [W/m^2]
$I_o(\theta)$	Incident solar radiation around the cylindrical surface of tube [W/m^2]
I_s	Scattered radiation [W/m^2]
I_t	The transmitted radiation intensity [W/m^2]
h_f	Convective heat coefficient inside receiver tube [W/(m^2 K)]
k	Thermal conductivity [W/m K]
K_e	extinction coefficient [1/m]
K_a	Absorption coefficient [1/m]
L	Length of collector [m]
Nu	Nusselt number [dimensionless]
Pr	Prandtl number [dimensionless]
$\emptyset$	Rim angle [deg]
q_f	The absorbed heat flux of nano-fluid [W/m^2]
q_{loss}	Heat flux to ambient [W/m^2]

r	Radius
Ra	Rayleigh number [dimensionless]
Re	Reynolds number [dimensionless]
T_{amb}	Ambient temperature [K]
T_{anul}	Receiver and glass cover Annuals temperature [K]
T_c	Glass cover temperature [K]
T_f	Fluid mean temperature [K]
T_i	Inlet temperature [K]
T_o	Outlet temperature [K]
T_r	Receiver temperature [K]
T_{sky}	Sky temperature [K]
u	Velocity [m/s]
U_L	The loss coefficient [W/m^2. °C]
θ	Circumference arc angle [deg]
w	Width of collector [m]
τ_g	Transmittance of glass [dimensionless]
Φ	The heat generated (internal heat source) [W/m^3]
ε_C	Receiver copper emittance [dimensionless]
ε_g	Glass emittance [dimensionless]
a	Thermal diffusivity [m^2/s]
α	Thermal expansion [1/K]
σ	Steven Boltzmann constant [5.6697 x 10^{-8} W/(m^2 K^4)]
η_{th}	Thermal efficiency [dimensionless]
ρ	Density [kg/m^3]
μ	Dynamic viscosity [Pa s]

LIST OF ABBREVIATIONS

PTC	Parabolic Trough Collector
CSP	Concentrated Solar Power
CFD	Computational Fluid Dynamics
DASC	Direct Absorption Solar Collector
UDF	User Defined Functions
FVM	Finite Volume Method
IASC	Indirect Absorption Solar Collector
NCPSC	Nanofluid-Based Concentrating Parabolic Solar Collector
NDASC	Nanofluid-Based Direct Absorption Solar Collector

Thesis Layout

This research has been published in the following conference:

● A. Hameed, W. Saad Alkhazraji, and M. Elmnefi, "*CONCENTRATED SOLAR COLLECTOR WITH DIRECT HEAT EXCHANGE USING TRIPLE COPPER TUBES*," presented at the Ulusal Isı Bilimi ve Tekniği conference 13-16 September 2017, Çorum , Turkey.

ABSTRACT

NUMERICAL AND EXPERIMENTAL PERFORMANCE OF CONCENTRATED SOLAR COLLECTOR WITH DIRECT HEAT EXCHANGE USING NONE-CIRCULATED NANOFLUID

AL-KHAZRAJI, Waqas Saad

Master, Department of Mechanical and Aeronautical Engineering

Thesis supervisor: Assist. Prof. Dr. Mohamed Salem Elmnefi

November 2017, 85 pages

In concentrated solar energy systems, a new technique for solar collectors has been developed. The parabolic trough solar collector is one of the most mature concentrated solar technologies, in which several studies have been conducted to increase thermal efficiency. The Direct Absorption Solar Collector (DASC) is a device that uses a modern technique to collect the radiation of solar energy, and as it is newly founded, there is little research available in this domain. In this research, a new configuration of direct absorption solar collector has been developed. In this configuration, non-circulating nanofluid absorbs the solar radiation when it is set within a glass tube. The absorbed heat is conveyed directly to circulating water flowing inside the copper tube submerged in the nanofluid. The model has been developed numerically by using the ANSYS FLUENT software for the nanofluid in the annular region, in the flowing water region and the copper tube which separates the two different fluids. Heat absorption of concentrated solar radiation that is reflected by a parabolic trough has been simulated as a heat source in the energy equation that is solved in the nanofluid zone. The results of the simulation showed that the efficiency of the solar collector reached 55.31%. The model was experimentally tested using a rig designed for this purpose under 400 W/m^2 intensity solar radiation on the day of testing. Numerical and experimental results were compared. The error percentage results ranged between 3.17% and 5.6%. The influence of changing the volumetric flow rate and the inlet water temperature on the efficiency and performance of the new

configuration model was also studied in addition to the effect of changing and testing the volume fraction of the nanofluid at 0.0%, 0.05% and 0.075% on the new configuration. In addition to that, a triple copper tube model was developed and compared with a single copper tube model for the same blockage ratio. The results show that the single copper tube model performed better.

ÖZET

DEVRİDAİM OLMAYAN NANO-SIVI KULLANARAK DOĞRUDAN ISI DEĞİŞİMLİ YOĞUNLAŞTIRILMIŞ GÜNEŞ KOLLEKTÖRÜNÜN SAYISAL VE DENEYSEL PERFORMANSI

AL-KHAZRAJI, Waqas Saad

Yüksek Lisans, Makine ve Havacılık Mühendisliği Bölümü

Tez danışmanı: Yrd. Doç. Dr. Mohamed Salem Elmnefi

Kasım 2017, 85 sayfa

Yoğunlaştırılmış güneş enerjisi sistemlerinde, güneş kolektörleri için yeni bir teknik geliştirilmiştir. Parabolik oluk tipi güneş kolektörü, termal verimliliği artırmak için birçok çalışmanın yürütüldüğü temel yoğunlaştırılmış solar teknolojilerinden biridir. Doğrudan Soğrulmalı Güneş Kollektörü (DASC), güneş enerjisinin ışınımlarını toplamak için modern bir teknik kullanan bir cihaz olup, yeni geliştirilen bir teknoloji olduğundan bu alanda çok az araştırma mevcut bulunmaktadır. Bu araştırmada, doğrudan soğrulmalı güneş kolektörünün yeni bir konfigürasyonu geliştirilmiştir. Bu konfigürasyonda, devridaim olmayan nano-sıvı bir cam tüp içine yerleştirildiğinde güneş ışınımını emmektedir. Emilen ısı, nano-sıvı içerisine batırılmış bakır boru içinde akan ve devridaim olan suya doğrudan iletilir. Model, halka şeklinde bölgedeki ve devridaim olan su bölgesindeki nano-sıvı için ve iki farklı sıvıyı birbirinden ayıran bakır boru için ANSYS FLUENT yazılımı kullanılarak sayısal olarak geliştirilmiştir. Parabolik bir oluk ile yansıtılan yoğunlaştırılmış güneş ışınımının ısı emilimi, nano-sıvı bölgesinde çözülen enerji denkleminde bir ısı kaynağı olarak simüle edilmiştir. Simülasyon sonuçları güneş kolektörünün verimliliğinin %55.31'e ulaştığını göstermiştir. Model bu amaçla hazırlanmış olan bir teçhizat kullanılarak test edileceği günde yoğunlu 400 W/m² olan güneş ışınımı altında deneysel olarak test edilmiştir. Sayısal ve deneysel sonuçlar karşılaştırılmıştır. Hata yüzdesi sonuçları %3.17 ila %5.6 arasında değişkenlik göstermiştir. Çalışmada ayrıca

hacimsel akış oranının ve giriş suyu sıcaklığının değiştirilmesinin yeni konfigürasyon modelinin verimliliği ve performansı üzerindeki etkisi ile nano-sıvının hacim oranının %0.0, %0.05 ve %0.075 olarak değiştirilmesi ve test edilmesinin yeni konfigürasyon üzerindeki etkileri araştırılmıştır. Buna ek olarak, üçlü bir bakır boru modeli geliştirilmiş ve aynı blokaj oranı için tek bakır boru modeli ile karşılaştırılmıştır. Sonuçlar, tek bakır boru modelinin daha iyi performans gösterdiğini ortaya koymuştur.

Anahtar Kelimeler: Nano-sıvı, Doğrudan Soğurmalı Güneş Kollektörü, Yoğunlaştırılmış Güneş Kollektörü, Hacim Oranı

CHAPTER ONE
INTRODUCTION

1.1 Introduction

The costs of fossil fuels and electricity have been increasing in recent years, making alternative and renewable sources of energy more attractive. The use of solar energy is vital to our society because it is plentiful and free, and because it has zero emissions of CO_2 [1, 2]. Solar energy is suitable for a large variety of energy needs, such as house heating [3], local hot water production [4], industrial heat [5], and the production of electricity in solar power plants [6]. There are many types of concentrated solar systems. However, our focus is on the parabolic trough solar collector due to the area which it covers in the power generation field. The Parabolic Trough Collector (PTC) is used in many applications, including heating fluids, electricity production and industrial processes. Nanotechnology has recently been introduced in this field, such that solar energy collection is undertaken by a new technique known as direct solar absorption. This technique is used in a new generation of solar energy collectors instead of the traditional method which absorbs solar radiation by the selective spectral coating of the metal tubes. In the new technology, solar radiation is absorbed by a nanofluid. This nanofluid is produced by mixing one or more than one kind of nanoparticle with the base liquid which flows inside the glass tube and then passes into the heat exchanger to convey the gained heat to a cold liquid. The addition of nanoparticles to the liquid will enhance the thermal properties of the liquid, which will improve the efficiency and performance of the solar collectors.

1.2 Statement of the Problem

Improving the performance of solar collectors to collect the largest amount of solar radiation is one of the most important goals for researchers. On the other hand, thermal resistance facing the transporter medium fluid is one of the main obstacles that reduces the performance and efficiency of a solar collector. The Direct Absorption Solar Collector (DASC) is the latest technology used in solar collection. In this system, a nanofluid passes through a glass tube instead of a mineral tube painted with spectral paint in the conventional system, whereas in a (DASC) the nanofluid absorbs solar radiation directly and transfers the absorbed heat energy to the heat exchanger for use.

Traditional thermal fluids, such as water, oil, ethylene/glycol propylene, etc., play a significant role in absorbing the solar irradiation in solar collector systems; however, these fluids have poor thermal properties compared to solid materials. Adding nanoparticles to these base fluids will improve their thermal conductivity [7] as solid nanoparticles such as Cu, Al_2O_3, CuO, Fe_3O_4, etc. have superior thermal conductivities [8]. The main goal of the research is to increase the harvest of solar energy by reducing the thermal resistance in the medium fluid, and to improve the efficiency of parabolic solar collectors by using the direct absorption technique and uncirculated nanofluid inside a glass tube which contains a copper tube submerged into the nanofluid as a direct heat exchanger.

1.3 Thesis Objective

There are two main objectives of this research. The first is to increase the total efficiency of the direct absorption solar collector system by using an uncirculated nanofluid. The second is to use the least amount of nanofluid, which in turn will reduce the cost of the system. In addition, heat transfer from the nanofluid into the system will be analyzed. We will examine the effect of using two concentrated nanofluids with volume fractions of 0.05% and 0.075%. The simulation will be performed on the ANSYS FLUENT software and an experimental setup was manufactured.

1.4 Significance of the Research

The new technique in this study used a stable nanofluid in order to increase the absorption of solar radiation rather than the flowing nanofluid used in the traditional system, as mentioned in the previous explanation. In our new system, we dispensed with the heat exchanger in the new configuration.

In the conventional system of a direct absorption solar collector (DASC), the nanofluid circulates and flows around the system and it absorbs solar radiation through a passage into a glass tube. The nanofluid absorbs the heat energy from solar radiation; then it conveys this heat to the cold water inside a heat exchanger. This heat is utilized to heat the water or for other applications as required. Conventional solar collectors require a large number of nanoparticles to produce the nanofluid in order for the nanofluid to flow inside the system and convey the absorbed heat to a heat exchanger, which increases the cost.

The new system in this study utilizes the direct heat exchange between non-flow nanofluid and circulated water inside the collector tube without the need for a heat exchanger. This will lead to a reduction of the thermal resistance. As a result, the total efficiency of the system will increase. Moreover, the system will use a single circulating pump rather than two because the nanofluid is uncirculated.

1.5 Organization of the Thesis

Chapter 1 includes the introduction and presents a statement of the problem, the thesis objective and the significance of the research.

Chapter 2 presents the previous studies that have focused on the collection of solar radiation in parabolic solar collector systems and the effect of using nanofluid in the field.

Chapter 3 presents the numerical and experimental methodologies in this thesis. The new design of the system presents the equations used to calculate the heat generated inside the nanofluid zone and thermal losses in a solar collector, as well as the experimental calculations of the new model. Furthermore, it shows the components used in the experimental setup for the new model.

Chapter 4 presents the results of simulations and experimental testing, with confirmation from tables and charts.

Chapter 5 contains the conclusion and future work.

CHAPTER TWO
LITERATURE REVIEW

Increased population growth and industrial progress in the world has caused an increase in the demand for electricity, as well as an increase in the cost and shortage of fossil fuels. All these reasons have led researchers to find alternative sources. Solar energy is one of these most important alternative sources because it is available, non-polluting and it has the capability of covering a wide variety of energy needs. The technology of Concentrated Solar Power (CSP) is the best system to collect solar radiation; it has the ability to supply energy for several fields including house heating, production of domestic hot water, industrial heat demands, and solar power plants for electricity production. According to Bellos et al. [9], there are four types of Concentrated solar power (CSP) systems that are use in the present time, namely the linear Fresnel reflector, parabolic trough concentrator (PTC), parabolic dish concentrator, and the heliostat field concentrator. Our study will be about the parabolic trough concentrator (PTC), which is the most common system. Moreover, it is considered a good investment in terms of cost and the possibility of integrating it with other energy sources, such as fossil fuels and other sources of renewable energy. There are many theoretical and experimental studies on the PTC, with the experimental studies outnumbering the theoretical. We have found that most researchers have focused their research on increasing the efficiency of PTCs at high operating temperature levels, reducing thermal losses, influencing of the mass flow rate of the working fluid and influencing the impact of placing the evacuated glass cover around the absorber tube. Other researchers have studied the thermophilic properties. In this chapter, we will review previous studies on the parabolic trough solar collector (PTSC). We will also look at nanofluids in solar collectors and the influences on thermophysical characteristics of adding nanoparticles to the base fluid.

2.1 Applications and Modeling of a Parabolic Trough Solar Collector

A parabolic trough solar collector system consists of a mirror in the form of a parabolic cylinder made of stainless-steel or aluminum plates which reflect the direct solar radiation to the receiver, which is placed at the focal point. The concentrated

solar radiation is transformed in the receiver into thermal energy and the heat transfer fluid absorbs it. Previous studies on the parabolic trough solar collector are presented as follows:

García et al. [10] carefully checked, with experimental data taken from Sandia National Laboratories, the numerical model using the finite element method (FVM). A numerical simulation for the thermal and fluid dynamic approach and the fluid of a single-pass parabolic trough collector was performed. The model was developed to include a double pass circulation of HTF. The results were enhanced in the heat transfer when the PTC was operated with external solar recirculation or with a double pass without recycling and thermal efficiency that could be enhanced compared with a single pass.

Öztürk et al. [11] studied the influence of geometry on PTCSs and the solar radiation incident to the surface of the reflector. The overall energy was also calculated inside the absorber tube. Moreover, the model was construed in relation to the energy and xerge models of meteorological specifications in different months in the city of Isparta in Turkey. The results showed that the highest value of efficiency was in July, where the highest intensity of solar radiation reached the highest rate in July. Moreover, the percentages were 76% and 27%, respectively.

Zheng et al. [12] studied the improvement of heat transfer for the solar receiver tube (PTC) by inserting a porous inside the tube with a non-uniform heat flux state. The new optimization technique was used to link the genetic algorithm and computational fluid dynamics in order to get optimal porosity formation. The results showed heat transfer performance examined through the porosity of the porous, Reynolds number and its thermal conductivity.

Kalogirou et al. [13] prepared a detailed thermal model showing all thermal analyses performed on a heat absorber tube for heat transfer operations, such as conduction, convection and radiation. Conduction was studied in an absorption tube through a metal tube and an envelope glass wall. They also studied the convection inside an absorption tube as well as inside the annular space between the vacuum tube and the absorption tube, and the outer diameter of the vacuum tube with the ambient air. Radiation from the outer diameter of the metal absorption tube and the surface of the envelope glass to the sky was also studied. The results of the thermal efficiency and losses were proven by comparing them with data from Sandia National Laboratories, and the results were deemed very satisfactory.

Tzivanidis et al. [14] devised a simulation model of the receiver tube that was carried out by the Solid Work program and based on the finite element method. A model of solar PCT was prepared and simulated for different operating conditions. The study aimed to estimate the efficiency of the model and to analyze each heat flux, distribution of the temperature in the receiver wall, and the phenomena of heat transfer occurring in the receiver tube. The final results showed that the PTC model performed efficiently. In addition, all computing was validated.

Padilla et al. [15] performed detailed calculations for the heat transfer into a parabolic solar collector trough by using a finite element method. A one-dimensional numerical simulation was used to analyze the PTC model. The absorption tube and the vacuum tube were divided into several sections, followed by the energy and mass balance being applied in each section as well as the convection and radiation heat transfer bonding in the calculations. The results of the model were compared with the Sanadiya National Laboratory results and with other models, and the simulation results demonstrated in terms of efficiency and thermal losses that the model in this study was better compared to the experimental results.

Ghasemi et al. [16] investigated the heat transfer properties of a parabolic solar collector with two segmental rings. The effect of the distance between two porous rings on the heat transfer coefficient of the collector was studied. The heat transfer fluid was Thermolin 66. The model was resolved by using computational fluid dynamics (CFD). The numerical simulation was performed for various distances between the two rings. The results showed that the use of two segmental rings in the solar absorber increased the heat transfer properties of the solar parabolic collector and by reducing the distance between the two segmental rings, there were increases in the heat transfer coefficient.

Al-Ansary et al. [17] introduced a promising technique to drastically reduce the gap between the cost and performance of a collector tube with an envelope glass tube that was filled with air or evacuated. They did so by placing the insulating material and heat resistant material inside the vacuum area between the absorber tube and the glass envelope in the receiver tube in the space that is not exposed to the concentrated solar radiation. It was predicted that the use of heat insulation materials would reduce thermal losses due to convection and radiation. The simulation results showed that losses from conduction and convection were 25% lower than in an air-filled tube when using fiberglass as thermal insulation. As the thermal conductivity of the insulation

material increased with increasing temperatures, it would reduce the utilization of thermal insulation applications which work at high temperatures. It was concluded that the proposed model could be a suitable alternative for low-temperature applications, with receivers that are discharged or filled with air.

He et al. [18] studied the effects of different geometrical concentration ratios and different rim angles on the distribution of the heat flux. An analysis of the concentrating characteristic of the PTSCs was made in two associated methods, Finite Volume Method (FVM) and Monte Carlo Ray Trace (MCRT). The results showed the two variable influences of heat flux distributions. Where GH increased, heat flux distributions became soft, and the angle extension of the limiting area becomes greater and the effect of shadows on the absorber tube becomes weaker. Moreover, when the rim angle increased, the maximum heat flux value lowered, and the curve moved towards the direction at the range of circle angle $\varphi = 90°$. However, the temperature rose only with the increase of the GC and the impact of the rim angle on the heat transfer process could be ignored when the rim angle was greater than 15°. If the rim angle had been small, such as when it equaled 15°, many rays reflected from the glass cover, and the temperature increase was much lower.

Mwesigye et al. [19] performed a three-dimensional analysis of the thermodynamics and thermal performance of a parabolic trough receiver. Their analysis included a determination of the heat flux on the receiver absorber tube using the Monte Carlo Ray trace method and the use of computational fluid dynamics to examine thermal and thermodynamic performance. Their analysis showed that the use of higher concentration rates increased the receiver temperature gradients and entropy generation ratio. For the rim angle less than 60°, the high heat flux peaks led to high-temperature gradients in the receiver absorber tube as well as high entropy generating average. The effect of the rim angles decreased the thermal performance of the receiver when the flow rates increased to above 8.55×10^{-3} m^{3}s^{-1} at every inlet temperature for any given concentration ratio.

2.2 Nanofluid

A nanofluid is a liquid that includes solid particles called nanoparticles of nanometer size. A nanofluid is prepared by scattering nanoparticles in a base fluid. The nanoparticles used in nanofluids are generally of metals, oxides, carbides or carbon nanotubes. The base fluids can be water, ethylene glycol, synthetic oil, thermal

oil, thermal oil or engine oil. Nanofluids have new characteristics that qualify them to be suitable for many systems in the heat transfer field. A nanofluid is superior in each thermophysical property and heat characteristic compared to conventional fluids. Therefore, nanofluids can enhance the output parameters of a system and so can be used in solar energy systems to collect solar radiation by increasing the amount of solar energy gathered. We will show in the next review the important effects of nanoparticles on the main thermophysical properties of the base fluid.

2.2.1 Thermophysical Properties of a Nanofluid

2.2.1.1 Thermal conductivity

Many experiments have been performed to examine the variation in thermal conductivity of nanofluids. The addition of nanoparticles to a conventional fluid raises its thermal conductivity. This is due to Brownian motion (Figure 2.1), which is the main factor controlling the thermal conductivity behavior of nanoparticles in fluid suspensions. The second effect is the interfacial layer (nanolayer), in which the molecules of the liquid (Figure 2.2) adjoining the surface of the solid particles forms layered structures. These layered structures become a thermal bridge between the nanoparticles and the bulk liquid and increase the thermal conductivity. [20]. Every study has shown that the thermal conductivity of nanofluids is higher than those of the base fluids. The measurement of the thermal conductivity of nanofluids can be performed following different techniques, such as by using the transient hot-wire apparatus, constants analyzer, or the hot disk thermal. The experiments and studies have been performed on different base fluids (water, ethylene glycol, methanol, propylene glycol, glycerol, engine oil, gear oil, paraffin, etc.) with various types of nanoparticle.
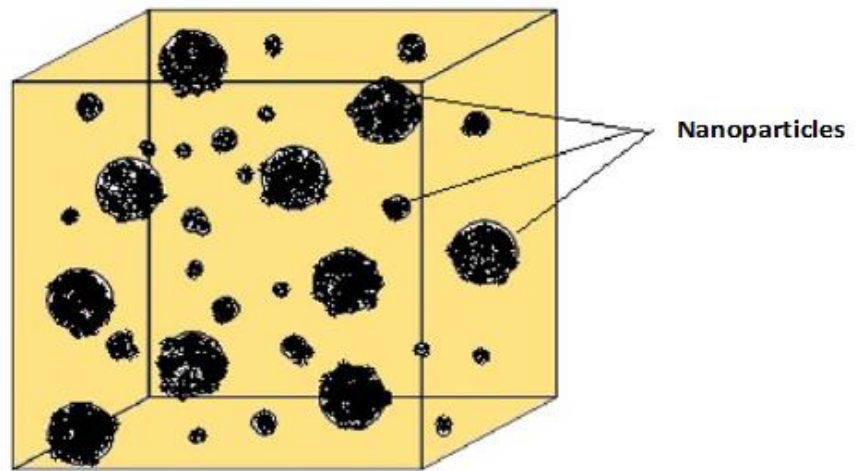
Figure 2.1: Brownian motion of nanoparticles [20].
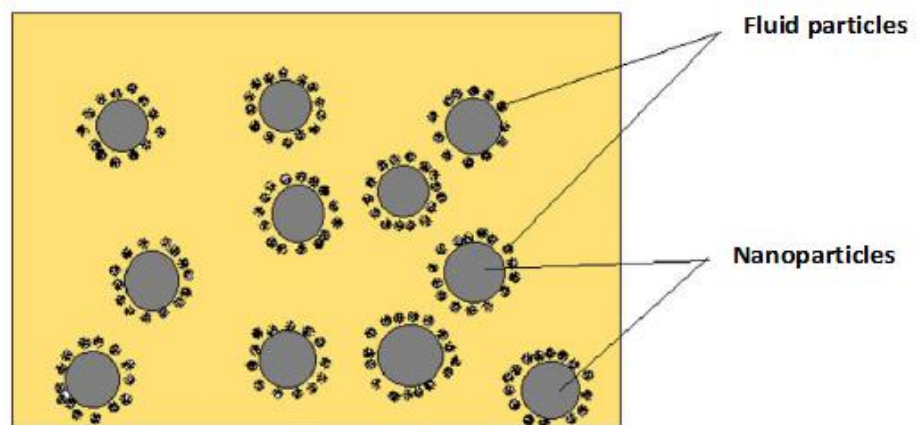
Figure 2.2: Nanofluid structure consisting of bulk liquid, and nanoparticles
nanolayers at the solid / liquid interface [20].

Liu et al . [21] conducted a study to improve the thermal conductivity for two
types of liquid, namely synthetic engine oil based multiwalled carbon nanotubes, and
ethylene glycol based multiwalled carbon nanotubes. It was found that increasing the
volume concentration of nanoparticles by 1% in ethyl alcohol led to increased thermal
conductivity of up to 12.4%, while the increase in the thermal conductivity of the
synthetic engine oil was 30% at the volume concentration of nanoparticles at a rate of
2%.

Yu et al. [22] developed a new simple technique to produce ethylene glycol based nanofluids that have graphene nanosheets. The results revealed that the thermal conductivity of the base fluid was enhanced considerably by adding graphene nanosheets, and increased the value of the thermal conductivity by up to 86% for 5.0% vol. graphene. The results were such that the two-dimensional geometry, high aspect ratio and hardness of graphene and graphene oxide demonstrated an impact on the thermal conductivity of nanofluids and assisted in increasing the thermal transport property of the suspend nanofluids.

Murshed et al. [23] used rod-shaped and spherical TiO_2 nanoparticles to prepare a nanofluid by dispersing the nanoparticles with deionized water. The experimental results produced an enhancement in thermal conductivity when increasing the nanoparticle volume concentration (0.5-5 vol.). Moreover, thermal conductivity was influenced by the size and shape of the nanoparticles. The results also showed that the thermal conductivity of TiO_2 (15 nm)–water, as a nanofluid, increased by 29.70% with a 5% volume concentration of nanoparticles, while the thermal conductivity of TiO_2 (10 nm $\times$ 40 nm)-water as a nanofluid showed a 32.8% increase in the same volume concentration of nanoparticles. Moreover, the shape of the nanoparticles affected the thermal conductivity. The rod-shaped particles showed more enhancements in the thermal conductivity compared to the spherical particles.

2.2.1.2 Viscosity

Viscosity is another fundamental parameter for applications of heat transfer, on which pressures fall and on which pumping power depends. Efficient viscosity depends on the viscosity of the conventional fluid used as a base fluid and the mass fractions of nanoparticles. In addition to these factors, the nanoparticles' diameter and temperature, as well as the type of nanoparticles, also influence the effective viscosity of nanofluids.

Kole et al. [24] investigated the viscosity of CuO-gear oil nanofluids. They demonstrated the influence of CuO nanoparticle weight fractions (0.005-0.025) and temperatures (10°C and 80°C) on nanofluids. The results showed that the viscosity of nanofluids with a CuO weight fraction of 0.025 improved the gear oil as a base fluid by almost three times, while it reduced significantly with an increase of temperature.

Arefmanesh et al. [25] in their study, inspected the efficient dynamic viscosity of Al_2O_3-water nanofluid depending upon the influences of uncertainties in the laminar

convection fluid flow and heat transfer in a square cavity. For this objective, two correlations, such as Maiga's correlation and the Brinkman formula, were used to find the dynamic viscosity of the nanofluids. The results were for these two models the Richardson number and the weight fraction of the nanoparticles. Their influences were examined in the flow field within the cavity. The impacts of the uncertainties in the dynamic viscosity formula of nanofluids very importantly depended on the Richardson number as well as on the weight fraction of the nanoparticles.

Moghaddam et al. [26] experimentally prepared a graphene–glycerol nanofluid to measure the properties of nanofluids. The results showed that the viscosity of graphene–glycerol nanofluids depended on the weight fraction and temperature. The viscosity rose with an increase in the weight fraction and dropped with a rise in temperature. In this study, a 401.49% improvement in the viscosity of glycerol was obtained with a weight fraction of 2% graphene nanosheets at a shear rate of 6.32 s^{-1} and 20°C.

2.2.1.3 Specific Heat

Specific heat is one of the important properties of nanofluids. It has a significant role in simulating the heat transfer rate of a nanofluid. The definition of specific heat here is the amount of heat required to increase the temperature of one gram of a nanofluid by 1°C. There are two specific heat types used in an investigation to determine the specific heat of nanofluids. The first type is based on the weight fractions of nanoparticles as proposed by Pak et al. [27]. The idea was taken from the liquid-particle mixture formula. The second type is based on the heat equilibrium technique as proposed by Xuan et al. [28].

Tiznobaik et al [29] investigated the specific heat of high-temperature dissolved salt-based nanofluids. Four various sizes of silicon dioxide nanoparticles (5, 10, 30, and 60 nm) were scattered in a molten salt eutectic to produce high temperature operating fluids. The measurement of the specific heat capacity of the nanofluids was carried out by several scanning calorimeters. The result was that the specific heat capacity of this nanofluid increased equally by 25% compared to the base fluid.

Yang et al. [30] used the mechanics method, to examine the molecular structure and specific heat of super carbon nanotubes. The results achieved were that the specific heat of the super carbon nanotubes had a stable value for a given temperature which was almost independent of the length and diameter of the super carbon nanotubes.

Robertis et al. [31] used a differential scanning calorimetry mechanism applied on a specific heat capacity to determine a good correspondence between gaining and tabulating the values of the components in nanofluids (copper and ethylene glycol as a base fluid). The results revealed that the presence of copper nanoparticles in the base fluid changed the characteristics of the crystallization and melting operations and decreased the specific heat values of the nanofluids in the total temperature range.

2.2.1.4 Density

Density is one of the important thermophysical properties which play a major role to estimate the heat transfer effectiveness of nanofluids. It directly impacts the Reynolds number, Nusselt number, friction factor, and pressure loss.

Pastoriza et al. [32] conducted an experimental investigation into three different nanofluids with a dispersal of various concentrations (0.5% to 7% in mass fraction) of Al_2O_3 nanoparticles in water as a base fluid. The density was measured at three temperatures (283.15°K, 298.15°K, and 313.15°K), and the pressure range (atmospheric reaching to 25 MPa). It was observed that the effects of smaller particles on the volumetric behavior were very apparent. Although the comprehensive effect of size appeared to be small. The density rose with the concentration of nanoparticles. The variation from the equation for the smaller sized nanoparticles was compared with the two models; the density was increase with smaller nanoparticles. Limited data were obtainable in the literature for the density measurement of nanofluids, especially in ethylene glycol/water base fluids.

Singh et al. [33] experimentally presented the density of a CuO/water nanofluid; however, the results were not compared with the equation. They predicted that the density was enhanced with the weight fractions, but reduced with the temperature.

Teng et al. [34] in an experimental study, calculated the density of an alumina (Al_2O_3)/water nanofluid. The results revealed that the divergence of the density with the equation drops within the range of 1.50%–0.06% and 0.25–2.53%, respectively. Moreover, the results of the density had a greater divergence as the particle weight fractions of the nanofluid increased. The two types of densities in the experimental results were obtained to be within the reasonable divergence range.

2.3 Types and Applications of Parabolic Trough Solar Collectors

There are two types of parabolic trough solar collector which harvest solar radiation. The first type is called an indirect absorption solar collector (IASC). In this model, solar radiation is absorbed by the spectral selected coating, which coats the surface of a metal tube receiver. The second type is called a direct absorption, usage of the nanofluid-based concentrating parabolic solar collector (NCPSC). In this model, solar radiation is absorbed by the nanoparticles found in the nanofluid as HTF inside a glass tube instead of by the metal tube.

2.3.1 Indirect Absorption (IASC)

Sunil et al. [35] in an experimental study, examined parabolic solar collector performance using a SiO_2-H_2O-based nanofluid. The various volume flow rates taken were 20, 40 and 60 liters/hour. The concentration ratios of the nanoparticles taken were 0.01% and 0.05%. The manual tracking system was used to absorb the maximum amount of solar radiation. From the results, it was shown that the SiO_2-H_2O-based nanofluid produced a relatively higher efficiency at higher volume flow rates, and it increased the instantaneous efficiency with a rise in the volume flow rate. The maximum instantaneous efficiency was gained from the SiO_2-water based nanofluid (0.01% Vol. conc.) The volume flow rates for 20, 40 and 60 liters/hour were 10.45%, 21.55% and 30.48%, respectively. At 0.05% Vol. conc., the flow rates of 20, 40 and 60 liters/hour were 0.54%, 21.34% and 31.96%, respectively, as shown in Figure 2.3.
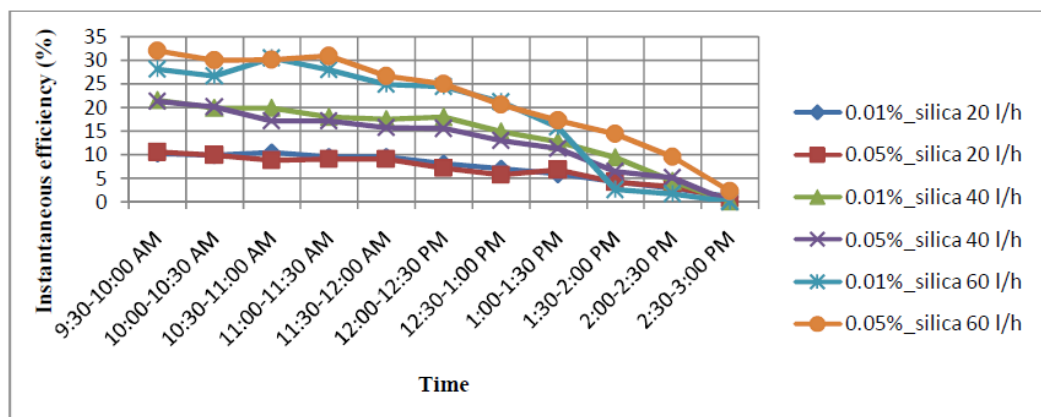
Figure 2.3: Contrast in instantaneous efficiency with time for SiO_2-water based on nanofluid (0.01% and 0.05% conc.) at varies volume flow rates [35].

Basbous et al. [36] conducted a numerical study on the thermal performance of the parabolic trough solar collector utilizing AL_2O_3-Syltherm 800 nanofluid as a working fluid. The numerical model used in this study was based on the energy balances of the solar collector and was supported by experimental data from the Sandia Laboratories in the USA. The results found that the nanoparticles significantly improved the convection coefficient between the receiver and heat transfer fluid and it was able to reduce heat losses by approximately 10%.

Ajay et al. [37] presented a study for both experimental and computational fluid dynamics, wherein a receiver consisting of two concentric cylinders (glass and absorber tube) with two fluid zones for the working fluid (internal cylinder) and a vacuum area (annulus). The nanofluid they used was 0.01% CuO-H_2O. The system performed under the mass flow rate of 20 liters/hour in the ANSYS FLUENT based computational fluid dynamics simulation. The absorption tube was constructed of copper with a working fluid flowing through it. The flow at the inlet was a uniform mass flow rate at an ambient temperature. The results from both the experimental work and the CFD analysis revealed that the thermal efficiency improved by 7.4% when 0.01% CuO/H_2O nanofluid was used, compared with conventional working fluids such as water at a flow rate of 20 liters/hour. The outlet temperature of both the experimental and the CFD were found to be in close agreement for the 0.01% CuO/H_2O nanofluid and 8.12% with a difference in the flow rate of 20 liters/hour, as shown in Figure 2.4.
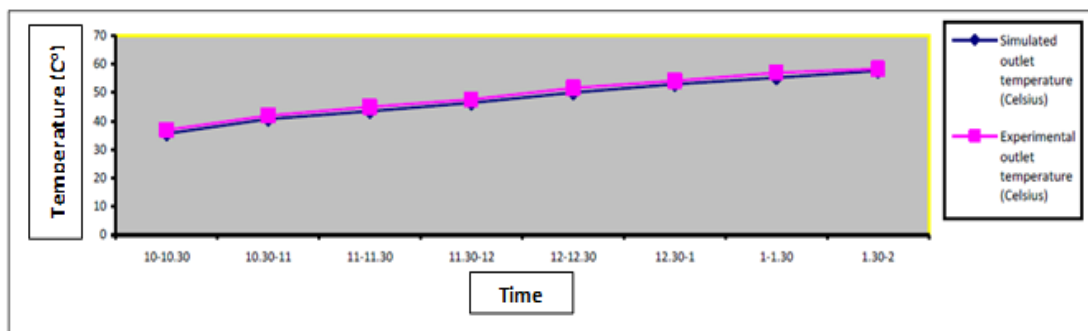
Figure 2.4: Computational and experimental outlet temperature varies with water at flow rate of 20 liters/hr [37].

Mwesigye et al. [38] performed a numerical study on, and presented results of the thermal and thermodynamic performance of a high concentration ratio for a parabolic trough solar collector by using Cu-thermal VP-1 nanofluid as a heat transfer fluid. The thermophysical properties of both the VP-1 oil and the copper nanoparticles were determined by the temperature. The inlet temperatures ranged from 350°K to 650°K and the flow rates in the domain ranged from 1.22 m³h⁻¹ to 135 m³h⁻¹. The numerical analysis depended on Monte-Carlo's ray tracing side-by-side with a computational fluid dynamics process, and their results indicated that the heat transfer performance of the receiver was enhanced with an increase in the volume fraction of the nanoparticles in the base fluid. Heat transfer performance increased by 8%, 18% and 32%, with an increase in the nanoparticle volume fractions from 0% to 2%, 4% and 6%, respectively, in addition to an increase in the Reynolds number as seen in Figure 2.5. Moreover, thermal efficiency rose to 12.5% when the volume fraction was 6%. Considerable improvements in thermal efficiency were achieved at low flow rates and low Reynolds numbers, as shown in Figure 2.6.
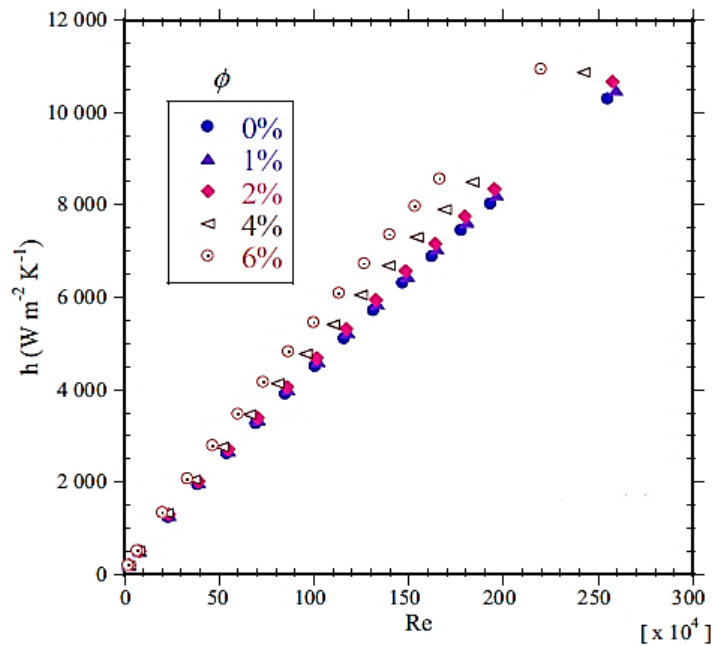
Figure 2.5: Performance of heat transfer as a function of the Reynolds number and the volume fraction of nanoparticles [38].
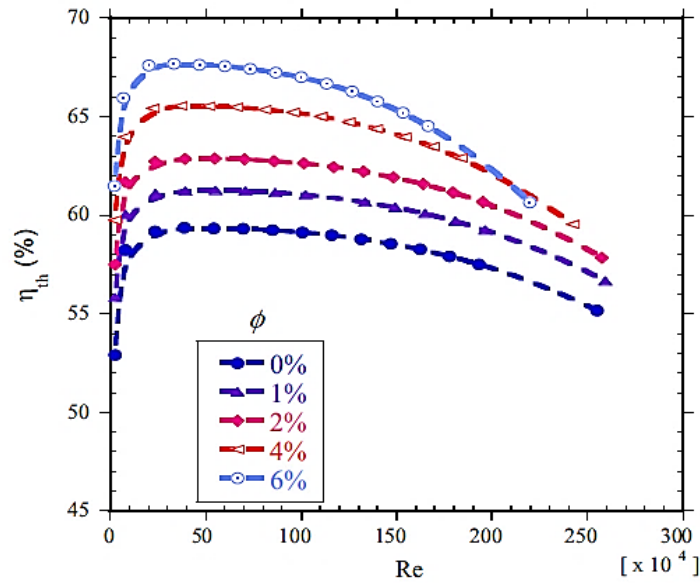
Figure 2.6: Thermal efficiency as a function of nanoparticle volume fraction and Reynolds number [38].

Kaloudis et al. [39] presented a study of numerical model results for the parabolic trough collector system with a Syltherm 800/Al_2O_3 nanofluid as a heat transfer fluid. It was found that the two-phase approach had an advantage in terms of precision, as opposed to a one-phase approach. As expected, the presence of nanoparticles promoted the heat transfer and increased collector efficiency. This increase was related to detailed temperature and velocity fields, demonstrating improved mixed convection influences for higher concentrations of nanoparticles. Even a 10% increase in efficiency was possible to concentrate the Al_2O_3 at 4%. The result was compatible with previous relevant studies that had found improvements of this magnitude by using nanofluids in a parabolic trough collector.

Kristiawan et al. [40] in an experimental examination, carried out a study of the thermal performance of TiO_2/distilled water as a nanofluid in the receiver tube with an evacuated glass cover with 0.1% volume concentration of titanium nanoparticles. In this parabolic trough solar collector system, the result was that an increase of heat transfer for the evacuated and non-evacuated conditions was 21.7% and 17.9%, respectively. The thermophysical properties of nanofluids changed mainly when adding nanoparticles to the base fluid, which was responsible for increasing the heat

16

transfer. The result of this work was that the evacuated case in the receiver tube was more efficient than the non-evacuated case.

2.3.2 Direct Absorption (NCPSC)

Ladjevardi et al. [41] in their study, investigated nanofluids in the direct absorption of solar radiation in a volumetric solar collector. The equations of radiation and transport are accompanied by the mass. The various diameters and volume fractions of the graphite nanoparticles were inspected for each condition. The efficiency of solar receivers was studied and the influence of the absorption of solar energy on the collected solar energy was analyzed, in addition to studying the radiation spectrum distribution and radiation energy levels with the depth of the flow. The results showed that by using graphite nanofluids at a volume fraction of 0.000025%, it will absorb more than 50% of the incident radiation energy at an estimated $0.0045 per liter increase in cost, while the maximum absorption of pure water in same solar collector would absorb only 27% of the incident radiation energy.

Menbari et al. [42] prepared and designed an experimental study, to examine the absorption and thermal conductivity of binary nanofluids. Binary nanofluids are a new category of nanofluids that include the base fluid and two different types of nanoparticle. Two different nanoparticles, namely CuO, which has high absorption properties and Al_2O_3, which has high scattering properties, were selected to prepare the binary nanofluid. Moreover, experiments with a NDASC collector found that the thermal efficiency of the system can be increased by increasing the volume fraction of nanoparticles (as shown in Figure 2.7) as well as the efficiency at different concentration ratios and various flow rates.
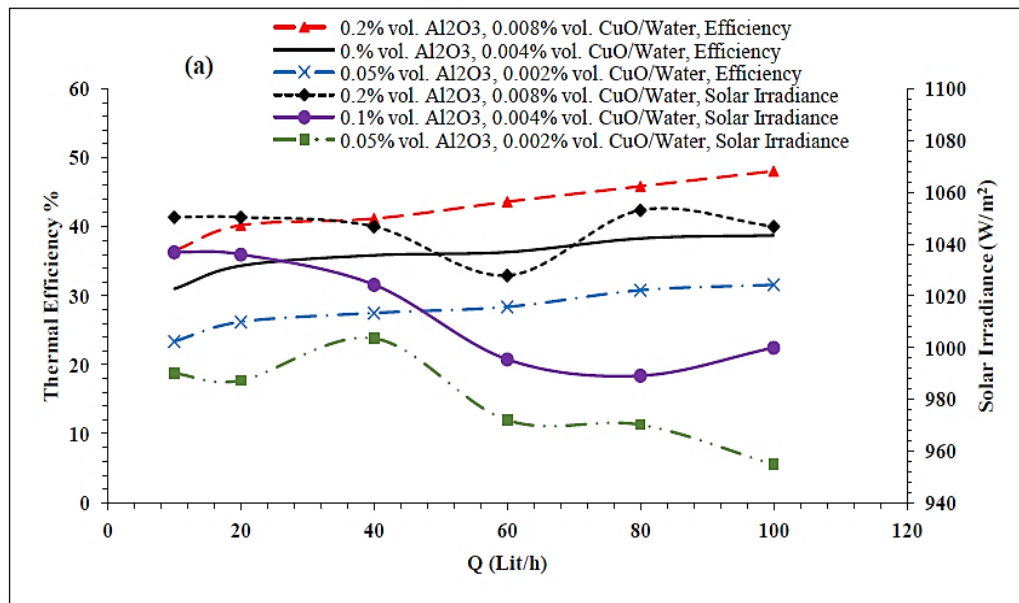
Figure 2.7: The efficiency at different concentration ratio and various flow rate [42].

Xu et al. [43] proposed an NDASC study using a nanofluid as a working fluid with a parabolic trough solar collector for medium-temperature solar collection. Operational properties were compared with conventional IASC through both theoretical analysis and experiments. A CuO/synthetic oil nanofluid was prepared and used as the working fluid for the NDASC. The nanofluid contained spherical CuO nanoparticles at a mass fraction of 0.055 wt.% and a size of 200 nm. The main results of this study were that by adding the nanoparticles, the absorption coefficient of the heat transfer fluid was greatly improved, as shown in Figure 2.8.
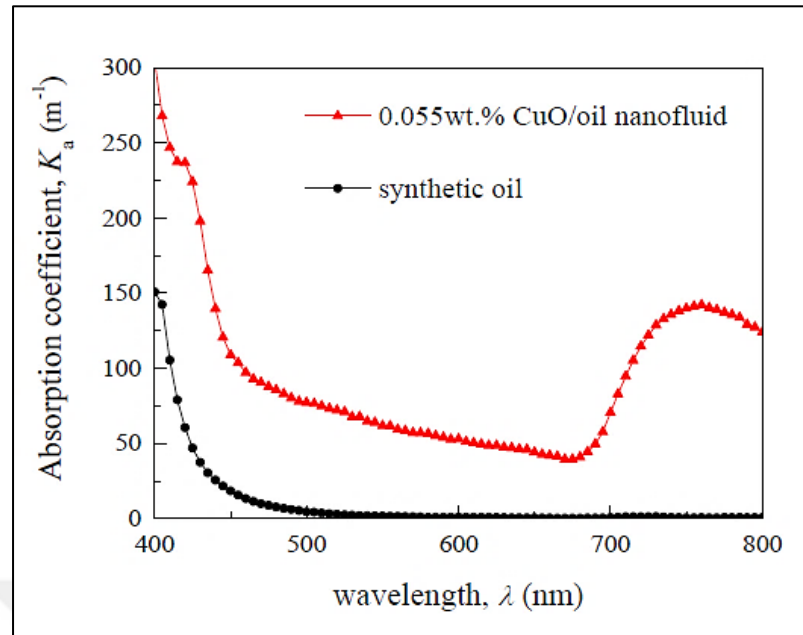
Figure 2.8: Absorption coefficient varies with wavelength for both nanofluid and synthetic oil [43].

The heat transfer in the NDASC uncoated glass tube was more efficient than the heat transfer in the IASC coated tube. The fluid temperature distribution in the tube cross section of the NDASC was more uniform than the IASC. For the conventional ISAC with solar concentration, the maximum temperature occurred on the tube wall, and the temperature in the focal lines was much higher, in contrast to the temperature of the nanofluid inside the uncoated glass tube being higher than the temperature of its wall under proven conditions for the NDASC. This can be explained by the fact that the solar radiation had been completely absorbed into the wall surface in the IASC, while the solar radiation had been transferred and absorbed by the nanofluid gradually through the layers in the NDASC (Figure 2.9).
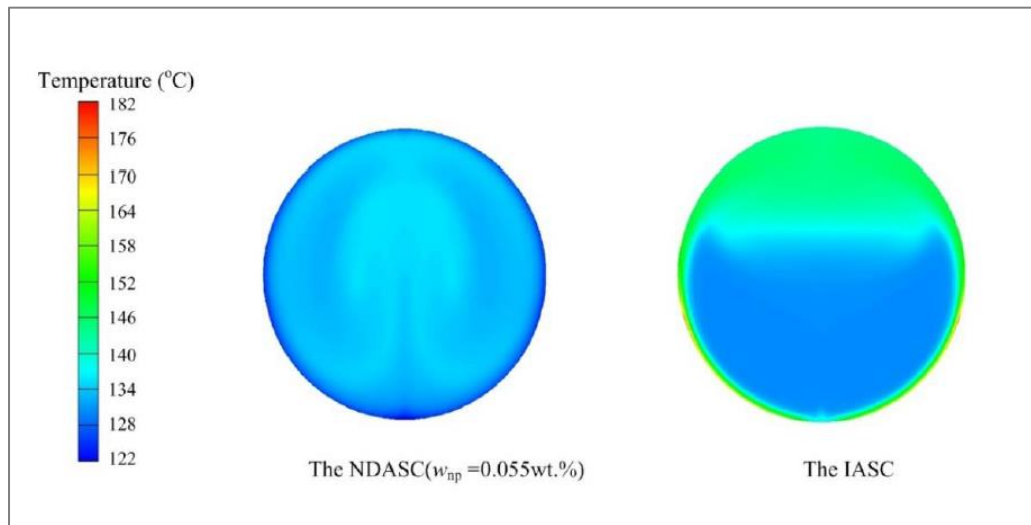
Figure 2.9: Distribution of fluid temperature at z = 1.7 m in NDADC and IASC (T_{fi} = 130° C) [43].

Resulting, the heat diffusion was more efficient inside the nanofluid and thus the distribution of the fluid temperature was more uniform in the NDASC. Moreover, the average nanofluid temperature at the outlet was higher. As a result, the efficiency of solar energy collection was universally higher.

Khullar et al. [44] studied and presented the idea of harvesting solar radiation energy with nanofluid-based direct concentrated parabolic solar collectors (NCPSC). For theoretical analyses of the NCPSC, a mathematical model was created, and the governing equations were solved numerically using different techniques. The results of the study were compared with the experimental results of traditional concentrated parabolic solar collectors under the same conditions. It was found that by maintaining the same external conditions (such as ambient/inlet temperatures, wind speed, solar insolation, flow rates, concentration ratios, etc.) that the NCPSC had between 5 and 10% higher efficiency compared with the conventional parabolic trough solar collector. Moreover, parametric studies were undertaken to determine the influence of different parameters on efficiency and performance. The following parameters in this study were studied: the convective heat transfer coefficient, solar insolation, and incident angles. The theoretical results obviously indicated that the NCPSC had the potential to collect solar radiation energy more efficiently than a conventional parabolic trough collector.

20

Chen et al. [45] performed a numerical study on the solar collector properties of the NDASC with the parabolic trough solar collector using a CuO/oil nanofluid with different concentration ratios of copper oxide nanoparticles of 0.05%, 0.06%, 0.075% and 0.1%, which were prepared and used as working fluids in NDASC. The operating characteristics of NDASC were simulated using the developed heat transfer model. The effects of the weight concentration of the nanoparticles on the heat transfer properties in the ADASC were analyzed and the optimal weight concentration used for the NDASC was obtained. The major conclusions were as follows: the distribution of fluid temperatures inside the DANSC tube was more uniform compared to the IASC. Furthermore, with the reduced nanoparticle weight concentration, the distribution of fluid temperatures becomes more uniform. Additionally, the weight concentration of nanoparticles had an effect on efficiency and critical temperature. The optimal weight concentration of the nanofluid for NDASC was between 0.05% and 0.06%.

CHAPTER THREE
SIMULATION AND EXPERIMENTAL STUDY

3.1 Introduction

The Direct Absorption Solar Collector (DASC) is a new apparatus that collects solar radiation and converts it into thermal energy. Instead of utilizing a metallic receiver tube painted with a spectrally chosen coating to absorb he solar radiation and to transfer the heat to the working fluid inside the tube. However, in indirect absorption, the flow of nanofluid in the glass tube absorbs solar radiation directly and transfers the absorbed heat energy to the heat exchanger so as to benefit from it. The nanofluid simultaneously plays two important roles with the dispersed nanoparticles inside it. These roles are the absorption of solar radiation and the transferal of the heat generated. Although a DASC is a new apparatus, there are many numerical and experimental studies on these collectors in which they are compared in terms of performance with the conventional solar (IASC) device. The traditional direct absorption parabolic trough solar collector consists of the main parts: the reflector, receiver, and heat exchanger. The significant component of the system is the receiver, which is manufactured from glass such as Quartz or Pyrex, as seen in Figure 3.1. A traditional DASC system contains a separated heat exchange. Solar radiation passes through the glass and is absorbed by the nanofluid flowing into the glass tube, followed by the temperature increasing rapidly, as seen in Figure 3.2. Here, the nanofluid transports the absorbed heat to the cold water inside a heat exchanger.
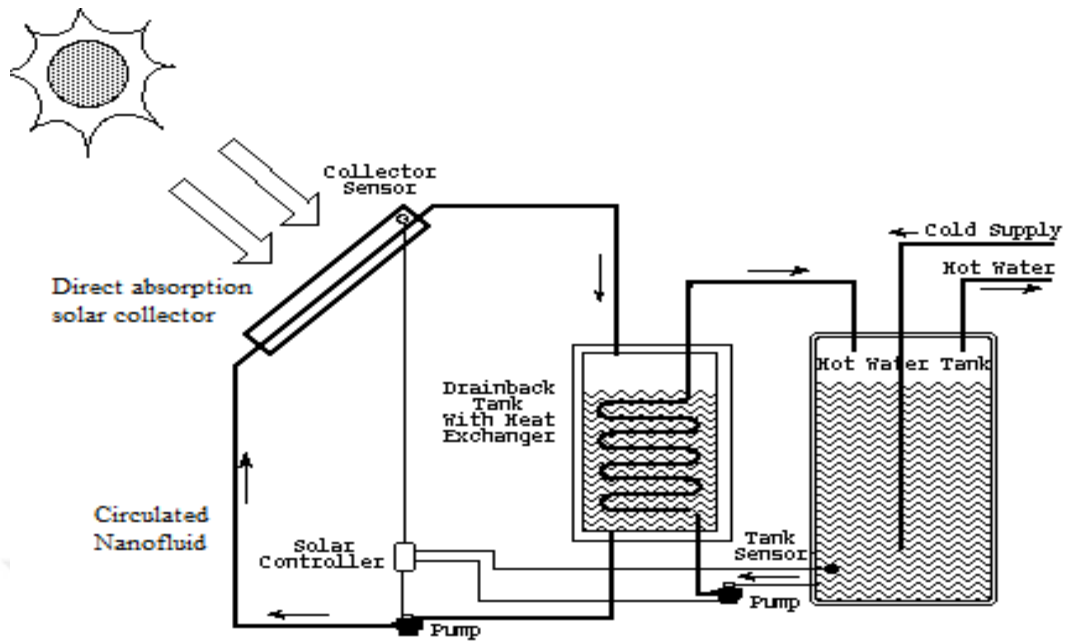
Figure 3.1: Conventional system of (DASC) with indirect heat exchange.
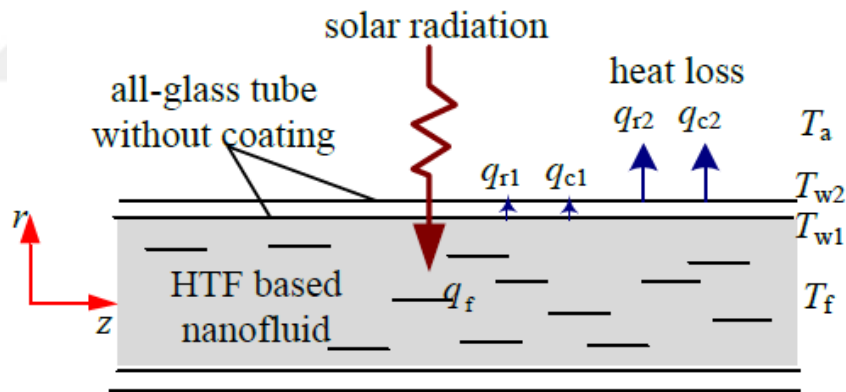
Figure 3.2: Receiver glass tube of direct absorption.

Losses in the traditional solar collector are due to the reflecting glass surface as well as the hot emissions from surfaces and convection losses. Furthermore, the heat produced by the system relies on the thermal efficiency of the heat exchanger, where the heat is transferred from the nanofluid to the water. The separated heat exchanger minimizes the total efficiency of the system due to the existence of additional thermal resistance. We changed the design of the solar collector receiver in order to reduce the thermal resistance. The new design decreases the overall thermal resistance of the

23

system by merging the two most important actions in one place. The heat absorption and exchange will occur in one location at the solar collector to minimize the total thermal resistance, as seen in Figure 3.3. As a result of the thermal resistance reduction, the total efficiency of the system will rise. In addition, we will use one circulating pump instead of two. The system outlines of direct heat exchange are illustrated in Figure 3.4. The present collector works for solar radiation absorption and heat exchange between the nanofluid as the absorber and the circulated water as a transporter. Solar radiation passes through the glass walls and it is absorbed by the nanofluid, leading to an increase in temperature.
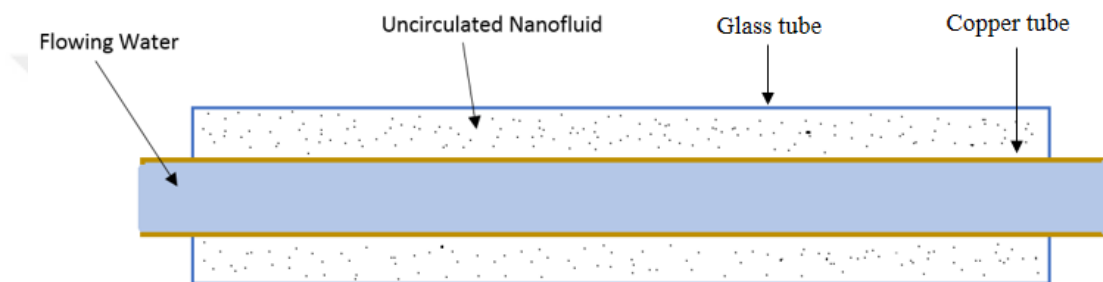
Figure 3.3: Receiver glass tube of the new model of direct absorption.
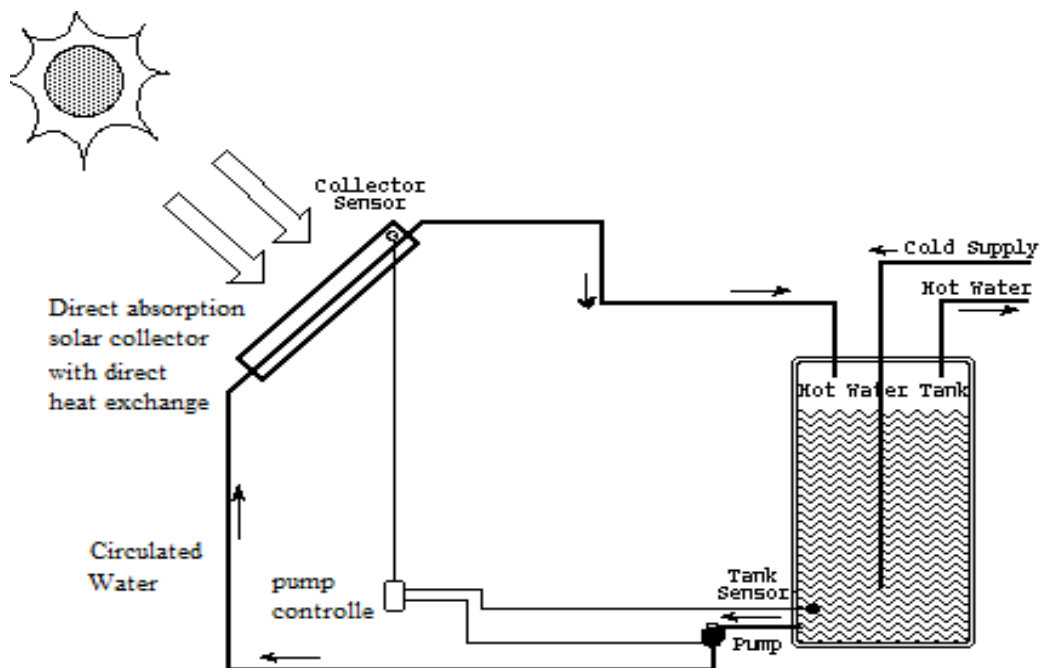
Figure 3.4: The outlines of the new system model with direct heat exchange.

The feasibility of this new technique of the direct parabolic solar collector for the glass and copper tube was determined for two different models to find the better of them. The first model used a single copper tube with a glass tube; the second model used triple copper tubes with a glass tube, where the triple copper tubes are equal in volume to the single copper tube in the first model. The two different models of the parabolic trough solar collector were simulated in ANSYS FLUENT. In the next sections, we explain the modeling equations and correlations utilized to calculate the new thermal properties of the fluid after adding the nanoparticles. Moreover, we present the equations which compute the heat generated inside the nanofluid due to solar energy absorption in addition to the modeling equations of the parabolic trough solar collector.

3.2 Designing the Models

The parabolic solar collector consists mainly of a reflector plate and an absorber tube. The absorber tube is located along of the focal line above the reflector and it is made of glass composite with the single copper tube (in the first model) and with a triple copper tube (in the second model) for direct heat exchange. The new approach employs a nanofluid instead of a spectral selective coating. This makes the absorber tube a heat exchanger to minimize the thermal resistance (see Figure 3.3). The receiver tube is the main part of the solar collector, and all thermal processes occur inside it. The dependent presumptions and constants in the simulation are:

1- The system works in a steady state condition.
2- Chemical and Thermal balance occur in all phases.
3- The fluid is on one phase.
4- The density of the water in the tube is constant.

The new model of the PTSC was simulated by performing a numerical simulation for a solar collector tube exposed to concentrated solar radiation with ANSYS FLUENT Figures 3.5 and 3.6 show the shape diagrams of a parabolic solar collector and how the radiation is reflected by the reflector surface onto the absorber tube.
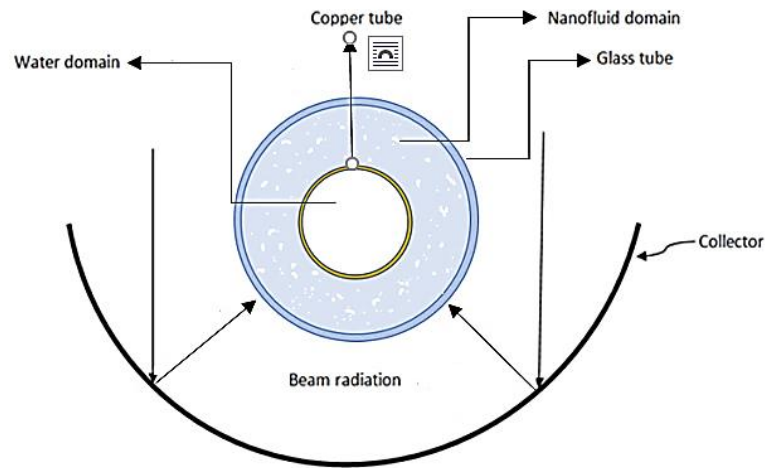
Figure 3.5: Parabolic trough solar collector with single copper tube.
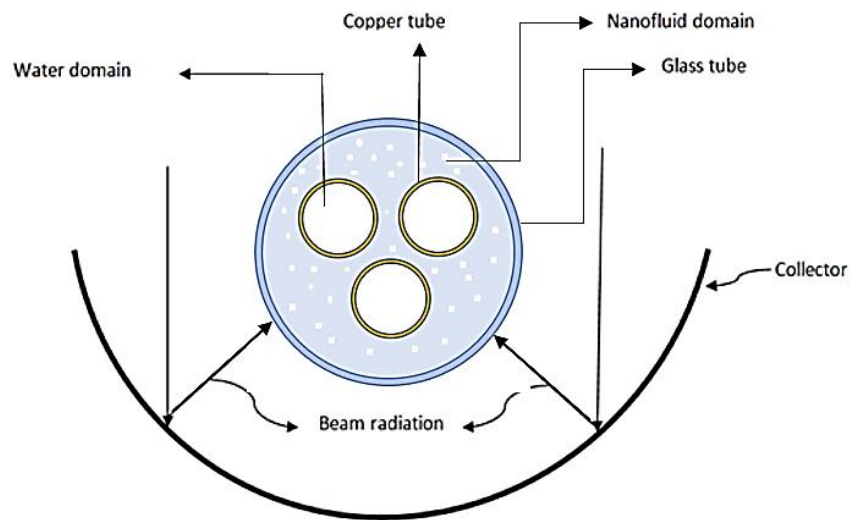
Figure 3.6: Parabolic trough solar collector with triple copper tubes.

3.2.1 Reflector

This part is the second main part of the parabolic trough solar collector, which influences the other main parts on it during sun tracking. It is generally made from a reflective metallic sheet in an arched form with the lowest absorption capacity onto a parabolic surface. The curve of the parabolic section must be with high accuracy to be

carried out geometrically, whereas that any deviation in the curve section will cause a deviation in the Solar radiation falling. Therefore, the reflected radiation must be in the direction of absorber tube to avert dispersion and ensure the concentration of radiation towards the receiver tube. For that, the equation of the parabola has been programmed with the Excel program, as appears in Figure 3.7. This is a model in the Excel program where the section coordinates and the required shape are calculated by depending on the design variables where the arc section of the parabola determined the angle and focal length. Figure 3.8 shows the definitive shape of the parabolic solar collector with its dimensions. These specifications of the parabolic trough solar collector are applied in the simulation as appears in Table 3.1.

Graphical Design of a Parabolic Trough Concentrator

Arc length = 1.21 m

Please enter the width : 1.050 m

Please enter the depth : 0.263 m

Focus = 0.262 m

Equation : Y = 0.95 X^2

Rim Angle = 90.0 °

X	Y	Angle	R from focus in m
0.000	0.000		
0.105	0.011	11.3	0.27
0.210	0.042	21.8	0.30
0.315	0.095	31.0	0.36
0.420	0.168	38.7	0.43
0.525	0.263	45.0	0.53
0.630	0.379		

In order to get depth to be equal to focus :

Width = 1.050 m

Focus = 0.263 m

Depth = 0.263 m

Figure 3.7: The program interface of the (PTSC) design using the Excel.
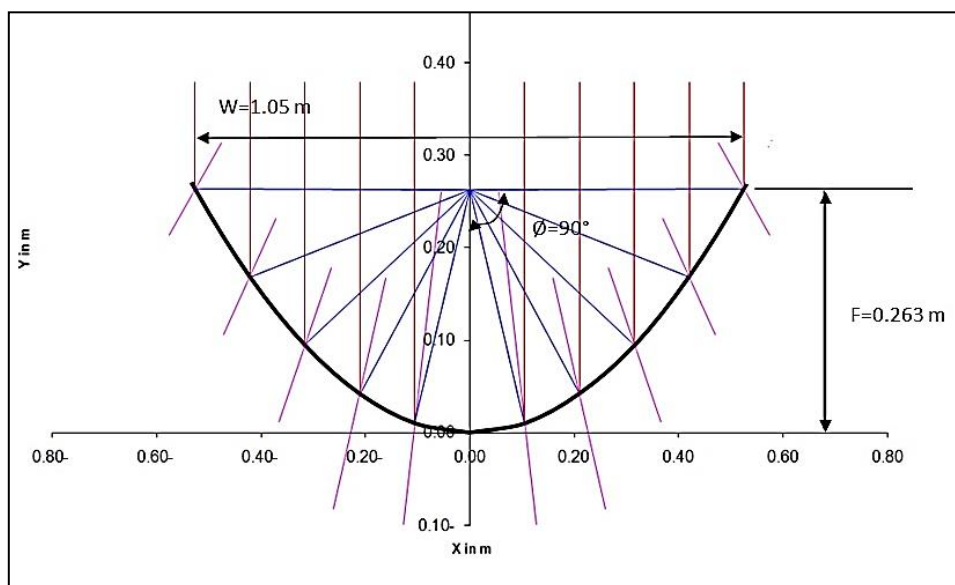
Figure 3.8: The definitive arc shape for the parabolic trough solar collector.

27

3.2.2 Receiver

The receiver of the parabolic trough solar collector includes the absorber tube which is placed in the focal point where the reflected rays are concentrated. Commonly, it is coated in black paint to gain the highest absorption of heat in the conventional solar collector. In this research, the geometric design of the receiver was changed by using a nanofluid instead the spectral selective coating. This was carried out by having the receiver consist of a glass tube composite around a copper tube and filling the gap between them with nanofluid (Figure 3.3). The water flows into the copper tube and nanofluid will be non-flowing inside the gap between the glass tube and the copper tube. The incident solar irradiation passes through the glass tube and is absorbed by suspended nanoparticles in the nanofluid and converted into heat energy rapidly. The heat energy generated inside the nanofluid will transfer to the flowing water through the copper walls. In the next section, the heat generated, convective heat transfer and thermal losses in the absorber tube are investigated. Table 3.1 shows the specifications of the parabolic solar collector utilized in the simulation.

Table 3.1: Receiver and collector properties.

Single copper tube (Receiver) at single model			
Variables	**Symbol**	**Value**	**Unit**
Material type	-	copper	-
Emissivity of copper	ε_c	0.07	-
Inner diameter	D_{ci}	22	mm
Outer diameter	D_{co}	25	mm
Triple copper tubes (Receiver) at tripl model			
Variables	**Symbol**	**Value**	**Unit**
Material type	-	copper	-
Emissivity of copper	ε_c	0.07	-
Inner diameter	D_{ci}	12.7	mm
Outer diameter	D_{co}	14.7	mm
Glass tube (Receiver) for two models			
Variables	**Symbol**	**Value**	**Unit**
Material type	-	Pyrex glass	-
Transmittance of glass	τ_g	0.93	-
Emissivity of glass	ε_g	0.89	-
Inner diameter	D_{gi}	51	mm
Outer diameter	D_{go}	56	mm
Material type	-	Pyrex glass	-
Collector (Reflector)			
Variables	**Symbol**	**Value**	**Unit**
width	w	1.05	m
length	L	1	m
Focal length	F	0.263	m
Rim angle	Ø	90°	deg
Material type	-	Stainless steel 430L	-
Optical efficiency	f	0.73	-
Concentrating ratio	C_R	6.55	-

3.2.2.1 Evaluation of Heat Generated

The absorber tube was subjected to simulation under steady state conditions. The heat generated in the nanofluid was calculated by utilizing theoretical calculation equations (to be explained later). Figure 3.10 illustrates the solar radiation transfer inside the nanofluid and the control volume. We assumed that the transmitted radiation intensity (I_t) change in only two dimensions (r, θ) in the cylindrical coordinate system, with no change of (I_t) along the z-axis. With reference to the Beer-Lambert Law, we can obtain the radiation intensity distribution in the receiver tube by utilizing the radiative transfer equation (Eq. (3.1)) [43]:

$$\frac{\partial I_t(r,\theta)}{\partial r} = -K_\ell I_t(r,\theta) \qquad (3.1)$$

where K_e is the extinction coefficient of the nanofluid, $I_t(r,\theta)$ the transmitted radiation intensity at coordinate (r,θ).

The incident intensity around the cylindrical surface of glass tube (I_o) is non-uniform and varies with the angle (θ) due to the form design of the collector; therefore, it was necessary to find an operation to calculate $I_o(\theta)$. Xu et al. [43] derived the next equation (Eq. 3.2) to calculate the radiation around the surface of the absorber tube. The equation was applied to the model and the results appear in Figure 3.8.

$$I_o(\theta) = 4 \, fG \, \frac{F}{D_{g0}} \, \frac{1-\cos\theta}{\sin^2\theta} \qquad (3.2)$$

where f is the optical efficiency factor and G the global solar radiation. We assumed G to be 400 W/m^2 in the simulation. (F) is the focal length of the parabolic trough collector which changes with the angle (θ). The angle (θ) ranges from $-75°$ to $75°$ due to the rim angle (Ø) being $90°$.

The transmitted radiation intensity at radius r I_t (r,θ), can be calculated with Eq. (3.3) [43].

$$I_t(r,\theta) = e^{-K_e r} I_0(\theta) \qquad (3.3)$$

There is some radiation that dissipates from the nanofluid; this is called the scattered radiation, I_s (r,θ), as seen in Figure 3.9. The absorption coefficient (Ka) is defined as a function of each $I_o(\theta)$, I_t (r,θ), and $I_s(r,\theta)$, as in the following equation (Eq. (3.4)) [43]

$$\frac{I_t\ (r,\theta)+I_s(r,\theta)}{I_o(\theta)} = e^{-K_a\,r} \tag{3.4}$$
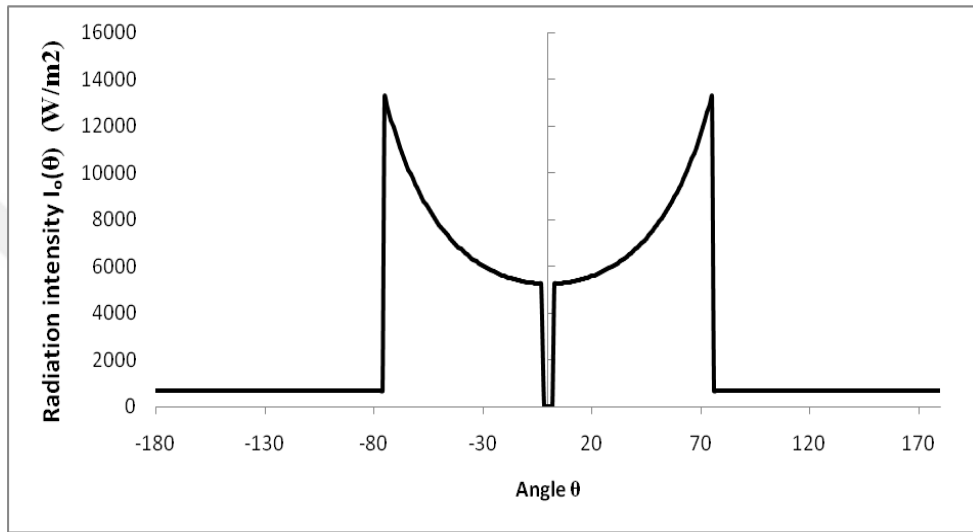
Figure 3.9: Intensity of reflected solar radiation around the receiver tube.

where the absorbed heat flux of the nanofluid $q_f(r,\theta)$ from the surface to the radius can be calculated by utilizing the absorption coefficient of the nanofluid in Eq. (3.5).

$$q_f(r,\theta) = I_0(\theta) - [I_t(r,\theta) + I_s(r,\theta)] = I_0(\theta)(1 - e^{-K_a r}) \tag{3.5}$$

The significant part of the aforementioned is how one can calculate the heat generated inside the nanofluid by utilizing the previous equations (from Eqs. (3.1) to (3.5)). The heat generated in the nanofluid is assigned as the internal heat source, and the relationship shows that the change occurs with optical depth towards the center of the tube. Therefore, the optical depth changes with the radius, where the relationship is:

$$\Phi = -\frac{\partial q_f}{\partial r} \tag{3.6}$$

31

The control volume was used for the purpose of deriving Eq. (3.6) for the generated energy inside nanofluid. The derived equation will be applied in the ANSYS software by creating a UDF (user-defined function) file as a thermal solar energy source in order to calculate the energy generated inside the nanofluid zone. The UDF applied in this study is listed in Appendix A. Figure 3.5 shows the control volume.

$$\Phi = -\frac{\partial q_f}{\partial r} = \frac{q_f(r_{i+1},\theta j)r_{i+1} - q_f(r_i,\theta j)r_i}{r_i - r_{i+1}} \quad (3.7)$$

Therefore, the heat transferred into the collector tube can be described mathematically with an energy equation and the internal heat source (Φ) inside the nanofluid, as shown in Eq. (3.8), as follows:

$$\frac{\partial(\rho u_x T_f)}{\partial x} + \frac{\partial(\rho u_y T_f)}{\partial y} + \frac{\partial(\rho u_z T_f)}{\partial y} = \frac{\partial}{\partial x}[\frac{k}{C}\frac{\partial T_f}{\partial x}] + \frac{\partial}{\partial y}[\frac{k}{C}\frac{\partial T_f}{\partial y}] + \frac{\partial}{\partial z}[\frac{k}{C}\frac{\partial T_f}{\partial z}] + \Phi \quad (3.8)$$
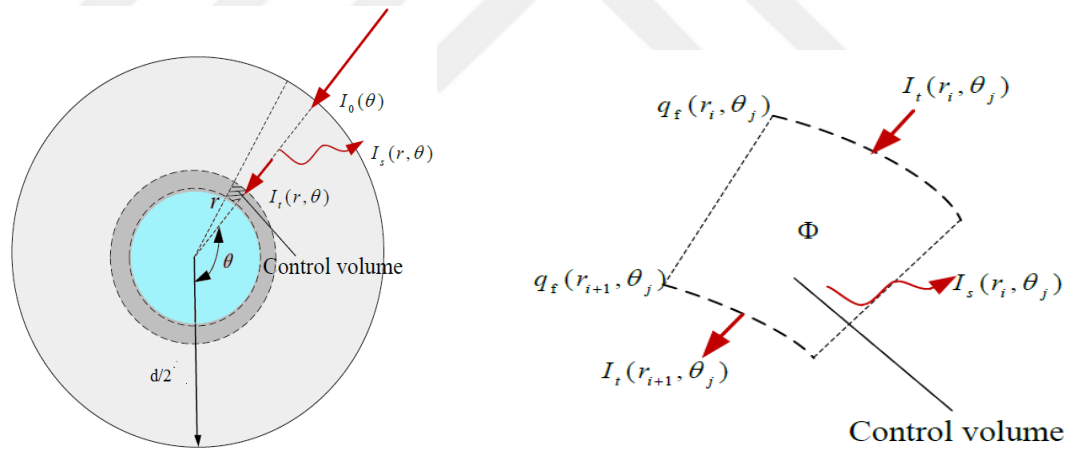
Figure 3.10: Solar radiation transmission inside the nanofluid tube and control volume properties.

3.2.2.2 Heat Transfer by Convection

As explained in the previous section, the heat generated inside the nanofluid was the result of the absorption by the nanoparticles of the reflected solar radiation. The nanofluid was not flowing, while the water was flowing and the temperature is unequal between the nanofluid and the copper tube. This will result in natural convection

between the nanofluid and the copper tube. The Rayleigh number is the parameter associated with the buoyancy-driven flow to compute the natural convection, and the Boussinesq approximation condition is the best process for solving the non-isothermal flow.

3.2.2.2.1 Rayleigh number

The Rayleigh number (Ra) is a dimensionless term utilized in the calculation of natural convection which relates to buoyancy driven flows. When the Rayleigh number is less than the critical specific value for a fluid, the heat transfer process will primarily be conductive heat transfer. When the Rayleigh number is higher than the critical value, there is a beginning of convective heat transfer. The case in this study is a copper tube enveloped by a glass tube and between them the nanofluid. The Rayleigh number calculated by utilizing Eq. 3.9, and the heat convection is calculated using Eq. 3.10 [46]. The two models were studied, as mentioned in Appendix B.

$$R_{aL} = \frac{g\beta(T_o - T_i)L^3}{\alpha v} \tag{3.9}$$

where R_{aL} is the Rayleigh number, β the thermal expansion coefficient, υ the kinematic viscosity and α the thermal diffusivity coefficient.

$$\bar{q} = \frac{2\pi\,k_{eff}}{\ln(r_0/r_i)}\,(T_0 - T_i) \tag{3.10}$$

where k_{eff} is the effective conductivity of the stationary fluid k_{eff} can be calculated with Eq. 3.11.

$$k_{eff} = 0.386\,k\left[\frac{pr}{0.861+pr}\right]^{0.25}\,(R_{ac})^{0.25} \tag{3.11}$$

3.2.2.2.2 Boussinesq Approximation

The Boussinesq approximation is a way to resolve non-isothermal flow, such as the natural convection problem, without having to solve the entire compressible formulation of the Navier-Stokes equation. The rule of approximation is that there is a flow, within which the temperature varies very little, and therefore, the density varies

33

very little, but within which the buoyancy drives the motion. Therefore, the variation in density is disregarded throughout except within the buoyancy term.

The problems occur when the fluid varies in temperature from one place to another, so the Boussinesq approximation is applied. When the temperature changes, it causes a flow of fluids and an increase in the heat transfer. In the Boussinesq approximation, the change in fluid properties is negligible, except for the density (ρ) that appears when multiplied by gravity. When u is the local velocity of a portion of the fluid, the equation of mass conservation becomes [47].

$$\frac{\partial \rho}{\partial t} + \nabla.(\rho u) = 0 \tag{3.12}$$

When disregarding the change in density,

$$\nabla.u = 0 \tag{3.13}$$

The Navier-Stokes equations is

$$\frac{\partial u}{\partial t} + u.\nabla u = -\frac{1}{\rho}\nabla p + v\nabla^2 u + \frac{1}{\rho}F \tag{3.14}$$

where $\nabla^2 u$ is the kinematic viscosity, and F is the forces.

$$\rho = \rho o - \beta \rho o \Delta T \tag{3.15}$$

when indemnity F = ρg, the equation will be:

$$\frac{\partial u}{\partial t} + u.\nabla u = -\frac{1}{\rho}\nabla p + v\nabla^2 u - g\alpha\Delta T \tag{3.16}$$

3.2.2.3 Computing Heat Losses

Heat loss is one of the most important problems highlighted in previous studies which we have attempted to reduce in order to have better efficiency. The thermal losses in the PTSC are calculated using Eq. (3.21) [48]. Because of the gradient at temperatures around the perimeter of the tube, the losses will vary from place to place on the surface of the tube. Therefore, a UDF file must be created to calculate the heat losses from the tube wall, and we adopt the value of Qloss to estimate the loss coefficient (UL) with Eq. (3.22).

$$Re = \frac{\rho a * Va * Dr}{\mu a} \tag{3.17}$$

The heat transfer coefficient for the wind (h_w) is calculated using Eqs. (3.18) and (3.19) [49], as follows:

$$Nu = h_w * D_{go} / \ k_w = 0.40 + 0.54 \ (Re)^{0.52}, \quad \text{If } (0.1 < Re < 1000) \qquad (3.18)$$

$$Nu = h_w * D_{go} / k_w = 0.3 (Re)^{0.6}, \quad \text{If } (1000 < Re < 50{,}000) \qquad (3.19)$$

$$h_w = K_w * Nu / D_{go} \qquad (3.20)$$

By substituting h_w into Eq. (3.21) to compute the heat loss with a 1-meter length:

$$Qloss = \pi \ D_{go} \ L \ h_w \ (T_r - T_a) + \varepsilon g \ \pi \ D_{go} \ L \ \sigma \ (T_r^4 - T_{sky}^4) \qquad (3.21)$$

$$U_L = \frac{Q_{loss}}{A_r \ (T_r - T_a)} \qquad (3.22)$$

where is εg is the glass emittance, σ the Stefan-Boltzmann, T_r the glass wall temperature, k is calculated using ANSYS FLUENT, T_a is the ambient temperature, T_{sky} the sky temperature $= T_a - 5$ (K), K_w the thermal conductivity of air, and A_r the receiver area.

3.3 Properties of Fluids

We used two types of fluids in this study. The first is a synthetic oil type (5W30) used as the heat transfer fluid. It was prepared as a nanofluid, and filled the gap between the glass tube and copper tube. The second fluid was water, which was utilized as a working fluid flowing into the copper tube.

3.3.1 Nanofluid

This part of the study presents the formulas that are used to calculate the thermal properties of the nanofluid. After completing the process of mixing the nanoparticles with the base fluid, we will produce a liquid with new properties which have been adopted in the numerical simulation. In this study, we used copper oxide (CuO) as nanoparticles and engine oil (5W30) as a base fluid.

3.3.1.1 Base Fluid Synthetic Oil (5w30)

This type of synthetic oil (5W30) was used for its low price and availability and for its high and long-term effectiveness. The operating temperature of the oil is 250°C. Therefore, it can work in two phases.

3.3.1.2 CuO Nanoparticles

The addition of nanoparticles to the base fluid enhances the thermal and physical properties of the heat transfer for fluids. These particles increase the value of the thermal conductivity coefficient, resulting in an enhancement of the efficiency of the heat transfer fluid. Moreover, it produces a change in the density and specific heat capacity. For our study, we selected 200 nm, spherical CuO nanoparticles.

The copper oxide (CuO) nanoparticles were selected for two reasons. The procedure of preparation of the nanofluid is simply due to the CuO consisting of copper joined with oxygen, and the existence of oxygen in the copper oxide assists the procedure of blending the nanoparticles with the base fluid. The second reason is the high thermal conductivity coefficient of copper oxide, which increases the thermal conductivity coefficient of the base fluid. 200-nanometer, spherical nanoparticles were selected for this study [45]. The thermophysical properties of the nanoparticles and the base fluid [50] at 27°C are presented in Table 3.2.

Table 3.2: Thermophysical properties for base fluid and nanoparticles.

parameter	Oil (5w30)	CuO	Unit
temperature	27	27	°C
μ	0.063	-	Pa.s
ρ	840	6300	$Kg.m^{-3}$
Cp	1900	475	$J.(kg.K)^{-1}$
k	0.14	33	$W.(m.K)^{-1}$
β	0.0007	$1.8*10^{-5}$	K^{-1}

3.3.1.3 Thermophysical Properties of Nanofluid

3.3.1.3.1 Thermal Conductivity of Nanofluid

In this study, we selected the Maxwell model [51] as it is used for spherical nanoparticles. For a minimum concentration ratio of 1%, the model is as follows:

$$k_{nf} = k_f \frac{k_p + 2k_f + 2\varphi(k_p - k_f)}{k_p + 2k_f - \varphi(k_p - k_f)} \qquad (3.23)$$

3.3.1.3.2 Dynamic Viscosity of Nanofluid

There are many models and equations to measure the dynamic viscosity of the nanofluids. In this research, we used the Einstein model [52] due to its being appropriate for spherical nanoparticles and minimum concentration of 2%. Moreover, the model was previously used to determine the viscosity of nanofluids. The model equation appears as follows:

$$\mu_{nf} = \mu_f (1 + 2.5\,\varphi) \qquad (3.24)$$

3.3.1.3.3 Specific Heat Capacity of Nanofluid

Specific heat capacity was calculated by assuming thermal equilibrium in the nanofluid between the copper oxide nanoparticles and the oil. It is calculated thus [53]:

$$C_{p\,nf} = C_{p\,p}\,\varphi + C_{pf}(1 - \varphi) \qquad (3.25)$$

3.3.1.3.4 Density of the Nanofluid

In order to estimate the density of the nanofluids, we assume that the homogeneous CuO nanoparticles and base fluid are a thermodynamically stable fluid. The formula used assumes a balanced case between the nanoparticles and the base fluid, applied by [53], as follows:

$$\rho_{nf} = \rho_f (1 - \varphi) + \rho_p\,\varphi \qquad (3.26)$$

3.3.1.3.5 Volume Fraction

The fundamental parameter of the nanofluid is the volume fraction. It is expressed as the concentration ratio of nanoparticles in the base fluid. The equation to count the volume fraction has been adopted from [54]. The volume fraction used in this study is 0.075%.

$$\varphi = \left[\frac{(\frac{W_{CuO}}{\rho_{CuO}})}{\left(\frac{W_{CuO}}{\rho_{CuO}} + \frac{W_{bf}}{\rho_{bf}} \right)} \right] \times 100 \qquad (3.27)$$

3.3.1.3.6 Thermal Expansion Coefficient

Thermal expansion is one of the physical properties which represent an important factor in many heat removal systems that include natural convection. The thermal expansion coefficient (β) of a nanofluid can be investigated with a formula obtained from [55]; thus:

$$\beta_{nf} = + (1 - \varphi) (\beta)_f + \varphi (\beta)_p \qquad (3.28)$$

3.3.1.3.7 Absorption Coefficient of the Nanofluid

The absorption of the solar radiation is the important main factor in the direct absorption solar collector. The addition of nanoparticles to the synthetic oil causes increased absorption of solar radiation compared to only synthetic oil [43]. The absorption coefficient (Ka) is the significant factor due to it being utilized in the computation of the energy generated inside the nanofluid, which we will see in the next section. It uses a spectrophotometer device to calculate the absorption coefficient.

The new properties were calculated after using the previous details from formulas and equations, and after adding the nanoparticles, with two concentration ratios of 0.05% and 0.075%, which will be applied in the simulation, as shown in Table 3.3:

Table 3.3: Physical properties of the nanofluid with two concentrating 0.05% & 0.075%.

Parameter	(CuO) nanoparticles	Synthetic oil (5w30)	nanofluid 0.0.05 wt.% CuO/oil	nanofluid 0.0.075 wt.% CuO/oil	Units
ρ	6300	840	1113	1249.5	$Kg.m^{-3}$
μ	-	0.063	0.070875	0.074812	Pa.s
k	33	0.14	0.16181	0.17358	$W.(m.K)^{-1}$
Cp	475	1900	1828.75	1793	$J.(kg.K)^{-1}$
Ka	-	2	75	214	m^{-1}
β	1.8×10^{-5}	7×10^{-4}	6.659×10^{-4}	6.4885×10^{-4}	K^{-1}

3.3.2 Water

Water has been used in many solar applications for heating. Heated water is used in domestic applications and in power plants where it is converted into steam. This happens when the water is flowing into the receiver tube of the parabolic trough solar collector, or when the oil flows inside the receiver tube and then passes it through the heat exchanger, which then heats the water inside the heat exchanger. In our study, water was used as a working fluid that flowed inside the copper tube, with various volumetric flow rates (20, 40, 60 and 80 liters/hour) and various temperatures (300°K, 315°K and 330°K). Where the water flows inside the tube, the convective heat transfer coefficient will be calculated by employing the correlations, as clarified in this section. The physical properties of water , which were used in the simulation are presented in Table 3.4.

Table 3.4: Physical properties of water with various temperatures [56].

Parameter	Inlet temperature of Water			Units
temperature	300	315	330	K
μ	9.1×10^{-4}	6.3×10^{-4}	4.9×10^{-4}	Pa.s
ρ	996.6	991.3	984.4	$Kg.m^{-3}$
Cp	4179.2	4179.4	4183.8	$J.(kg.K)^{-1}$
k	0.61	0.63	0.65	$W.(m.K)^{-1}$

3.3.2.1 Reynolds Number

The Reynolds number is used to examine whether the flow is laminar or turbulent and is symbolized by Re. The Re number is obtained by comparing the inertial force with the viscous force where an Re number above 4000 generally shows a turbulent flow. The equation of the Reynolds number is calculated with this equation:

$$Re = \frac{\rho . v . Dci}{\mu} \qquad (3.29)$$

3.3.2.2 Prandtl Number

The Prandtl number is a dimensionless number which is computed as the ratio of momentum diffusivity and the thermal diffusivity, thus:

$$Pr = \frac{\mu . Cp}{k} \qquad (3.30)$$

3.3.2.3 Nusselt Number

The Nusselt number is a dimensionless number which is calculated as the ratio of convective to conductive heat transfer. This number depends on the boundary and geometry of the surface, the flow type, the Reynolds number and the Prandtl number. Where the flow has been assumed laminar, the Nusselt number as obtained from [8] is calculated as:

$$Nu = 4.36 \qquad (3.31)$$

3.3.2.4 Convective Heat Transfer Coefficient

The total convective heat transfer coefficient of the fluid flowing through the absorber tube of a parabolic trough solar collector can be investigated by using following equation:

$$h = \frac{Nu . k}{Dci} \qquad (3.32)$$

3.4 Model Simulation

Computational fluid dynamics employs numerical methods and algorithms to solve equations of heat mass transfer and governing fluid flow. The commercial CFD package ANSYS FLUENT is utilized in this study. FLUENT is competent at analyzing a broad range of fluid flow problems, which include laminar and turbulent flows, compressible and incompressible flows, viscous and non-viscous flows, single-phase and multiphase flows, Newtonian and non-Newtonian flows, and so on. Moreover, both steady-state and transient analysis can proceed. In addition, FLUENT supplies solutions to problems of heat and mass transfer. Conduction and convection can be readily performed by adding an additional energy equation. The simulation has the ability to be carried out in 3D for the models. This section shows how to design and draw the model with the design modeler and how to generate the mesh using the mesh manager. In addition, it explains the governing equation utilized in ANSYS FLUENT to solve the model numerically.

3.4.1 Governing Equations

ANSYS FLUENT has the possibility to resolve fluid flow problems numerically by resolving governing equations. The equation of mass and momentum conservation have the ability to solve all flow types and flows included in heat transfer that can be solved in addition to the energy conservation equations [47].

3.4.1.1 Mass Conservation Equation

The mass conservation equation used in ANSYS FLUENT is:

$$\frac{\partial \rho}{\partial t} + \nabla.(\rho \vec{\upsilon}) = S_m \tag{3.33}$$

where S_m denotes the source term. It is added to the continuous phase from the dispersed second phase or user defined function sources.

3.4.1.2 Momentum Conservation Equation

The conservation momentum equation is solved in FLUENT, as follows:

$$\frac{\partial}{\partial t}(\rho\vec{v}) + \nabla.(\rho\vec{v}\vec{v}) = -\nabla p + \nabla.(\overline{\overline{\tau}}) + \rho\vec{g} + \vec{F} \qquad (3.34)$$

where $\overline{\overline{\tau}}$ is the stress tensor, p the static pressure, $\rho\vec{g}$ gravitational body force, and $\vec{F}$ the external forces, including user-defined source terms.

3.4.1.3 Energy Conservation Equation

The equation of energy conservation is as follows:

$$\frac{\partial}{\partial t}(\rho E) + \nabla\cdot(\vec{v}(\rho E + p)) = \nabla\cdot\left(k_{eff}\nabla T - \sum_{j}h_{j}\vec{J}_{j} + (\overline{\overline{\tau}}_{eff}\cdot\vec{v})\right) + S_{h} \quad (3.35)$$

where, k_{eff} is the effective conductivity, the first three terms on the right side are an expression of energy transfer due to conduction, species diffusion, and viscous dissipation, respectively, and $\vec{J}_{j}$ is the diffusion flux of species j. S_{h} is the volumetric heat sources we have defined as a user-defined function to compute the internal heat generated inside the nanofluid zone.

3.4.2 Finite Volume Method (FVM)

The finite volume method (FVM) is a numerical technique to represent and evaluate partial differential equations in the form of algebraic equations. In the finite volume method, the model is split into a number of cells and elements as a control volume because the variable of the benefit is evaluated in the centroid of the control volume. A volume integral is performed and converts the divergence case to a partial differential equation (Eq. (3.36)), into the surface integral (Eq. (3.37)) by utilizing the Divergence Theorem. The surface integral is then estimated as the flow at the surface of each control volume. The flow enters with a certain volume and it is equal to that leaving the adjacent volumes. Therefore, the FVM is inherently conservative in construction.

$$\frac{\partial u}{\partial t} + \nabla\cdot f(u) = 0 \qquad (3.36)$$

$$\frac{\partial}{\partial t}\int_{v}udx+\oint_{\partial v}f_{i}n_{i}ds=0 \qquad (3.37)$$

3.4.3 Buoyancy-Driven

When the model is dominated by a buoyancy force, such as natural convection, it can be resolved in ANSYS FLUENT with different methods, and which approximate the change in density with respect to temperature. For the nanofluid, the Boussinesq approximation is used considerably due to the comparatively rapid convergence rate. The model regards the density as a constant quantity in all governing equations to be solved except for the body force state in the momentum equation.

$$(\rho-\rho_{\circ})g \approx -\rho_{\circ}\beta(T-T_{\circ})g \qquad (3.38)$$

where ρ_{o} is the constant density of the flow, β the thermal expansion coefficient, and $T_{\circ}$ the operation temperature.

This approximation is valid when there is a small change in the density, $\beta \Delta T \gg 1$ [47].

$$\rho = \rho_0 (1 - \beta \Delta T) \qquad (3.39)$$

3.4.4 Selection of Solution Methods in the Simulation

The solver type, which could be used in the simulation, is pressure-based, and when used to solve the pressure-velocity coupling, there are four schemes that can be applied for calculation, namely SIMPLE, SIMPLEC, PISO, and coupled, where each option has the method in the solution. We used the coupled method in this study in order to provide high accuracy in the solution.

3.4.5 Theoretical Details in Simulation

The details of the numerical process used in the simulation, as appears in Table 3.5:

Table 3.5: Numerical processes used in the simulation.

Term	ANSYS FLUENT R15.0
The Viscous	Laminar
The Solver	Pressure-Based
Velocity – Pressure Coupling	Coupled
Time	Steady
Pressure	Second Order
Momentum	Second Order Upwind
Energy	Second Order Upwind
Gradient	Least Squares Cell Based

3.5 Design of Models

The ANSYS Design Modeler is an application utilized as a geometry editor with presence CAD models. Moreover, it is a parametric feature-based solid modeler of designs which can intuitively and rapidly begin drawing in 2D sketches, model 3D parts, and upload 3D CAD models of sketches in order to analyze the engineering preprocessing. This property was used to draw the two models. The XY plane was selected to draw the model using the sketch tool and the Boolean tool for sketching the 4 zones. Zone 1 shows the glass tube, Zone 2 shows the nanofluid area, Zone 3 shows the copper tube area, and Zone 4 shows the water area. Next, we used the extrude function to make the sketch 3-dimensional by utilizing both symmetric directions. We used the previous processes in drawing the two models requiring different designs. The first model used a single copper tube submerged into the nanofluid inside the glass tube, as shown in Figure 3.11. The second model used three tubes separated uniformly by an angle of 120° and submerged into the nanofluid inside the glass tube, where the centers of the copper tubes mediate the radius of the glass tube (Figure 3.12). The triple copper tubes are equal in terms of capacity to the single copper tube in the first model. In order to select the better model in terms of efficiency and performance, we ran numerical simulations. After running the simulations, it was found that the first model using the single copper tube was the better one in terms of the efficiency and performance, which we manufactured experimentally and adopted in the study. Table 3.6 shows the measurements used in the design of the two models. A 3-

dimensional model is a requisite because of its non-axial symmetry. However, a number of simplifications can be made. For example, one half of the first model will be used in the simulation because of the symmetry about the vertical plane passing through the tube axis. Figures 3.11 and 3.12 show the schematics for the receiver model geometry of the single copper tube and for the triple copper tubes, respectively.

Table 3.6: The dimensions of tubes used in two models.

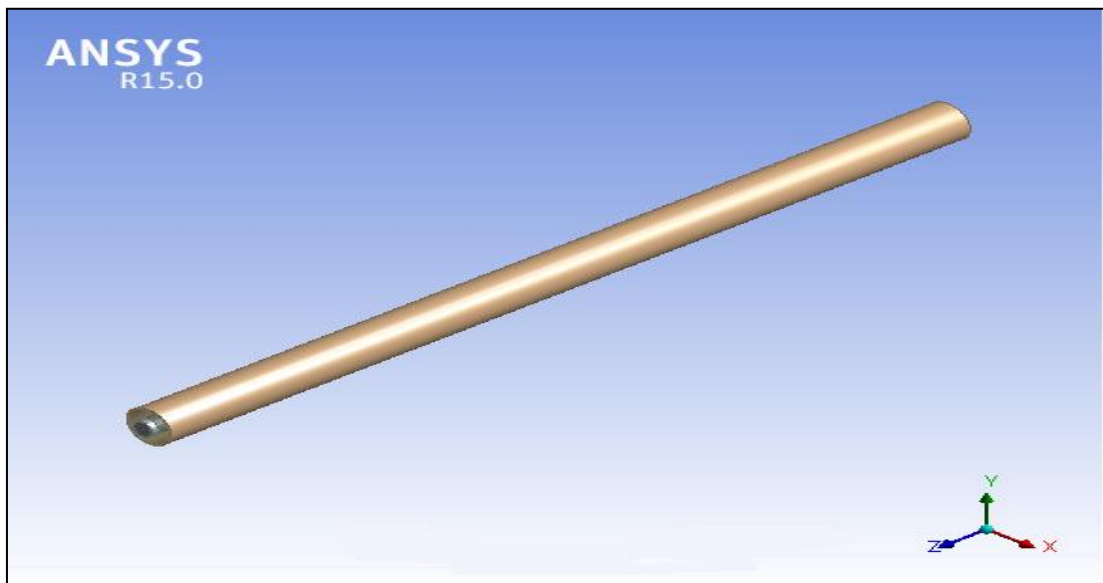| First model (Single copper tube)			
Material type	Inner diameter	Outer diameter	unit
copper tube	22	25	mm
Glass tube	51	56	mm
Second model (Triple copper tubes)			
Material type	Inner diameter	Outer diameter	unit
copper tube	12.7	14.7	mm
Glass tube	51	56	mm

Figure 3.11: Schematic diagram of the receiver for the single copper tube model.
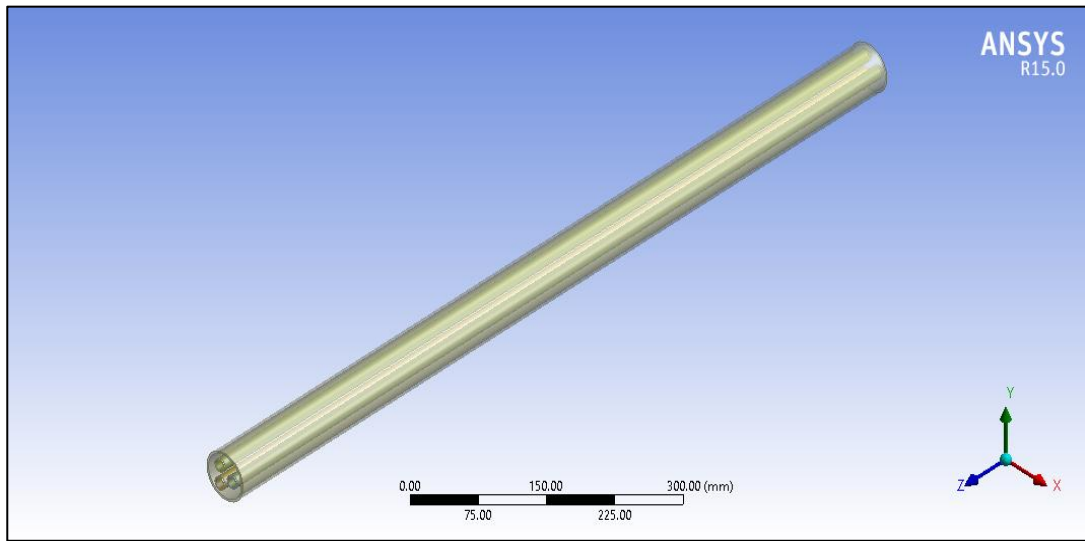
Figure 3.12: Schematic diagram of the receiver for the triple copper tube model.

3.6 Creating the Grid

The mesh is generated in a 3-dimensional model using the mesh manager in ANSYS for two models, as follows:

3.6.1 Triple Copper Tube Model

The number of cells was increased until the results became stable. The temperature rose for every one-meter change with the mesh cell number until it became stable at 5.3 million hexahedral cells (Figure 3.12). Critical changes of temperature and velocity near the walls needed a finer grid, especially in the water flow region. The *z*-axis represented the length of the tube, which was divided into 250 divisions (Figure 3.13). In Zone 1, the circumference of the glass tube was divided into 360 divisions. In Zone 3, the perimeter of the copper tube was segmented into 120 divisions for each copper tube. In Zone 2 for the nanofluid area, we applied a "face sizing" to divide it because the shape is irregular. In Zone 4, the water area also received a face sizing to divide it. In addition, the sweep method was applied to both the nanofluid area and the water area and make all of the parts compatible so as to avoid any divergence in the solution. Figures 3.13 and 3.14 show all details of the mesh.
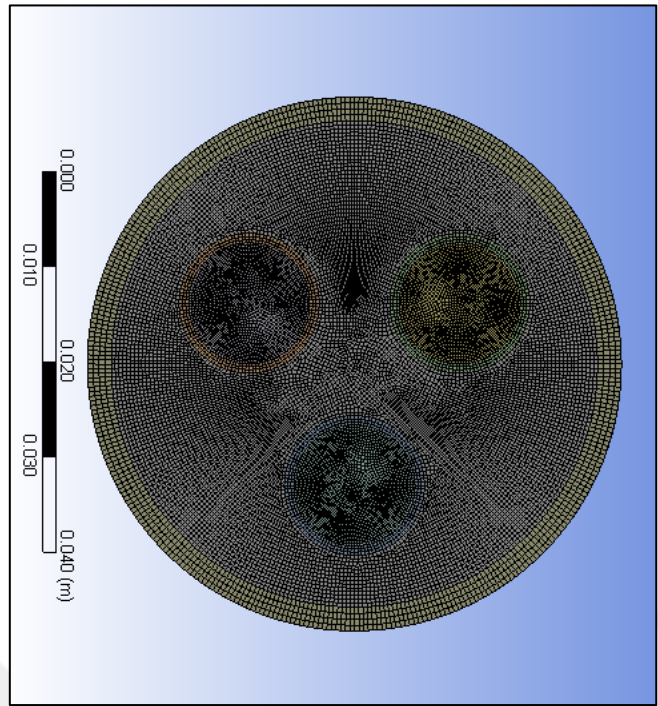
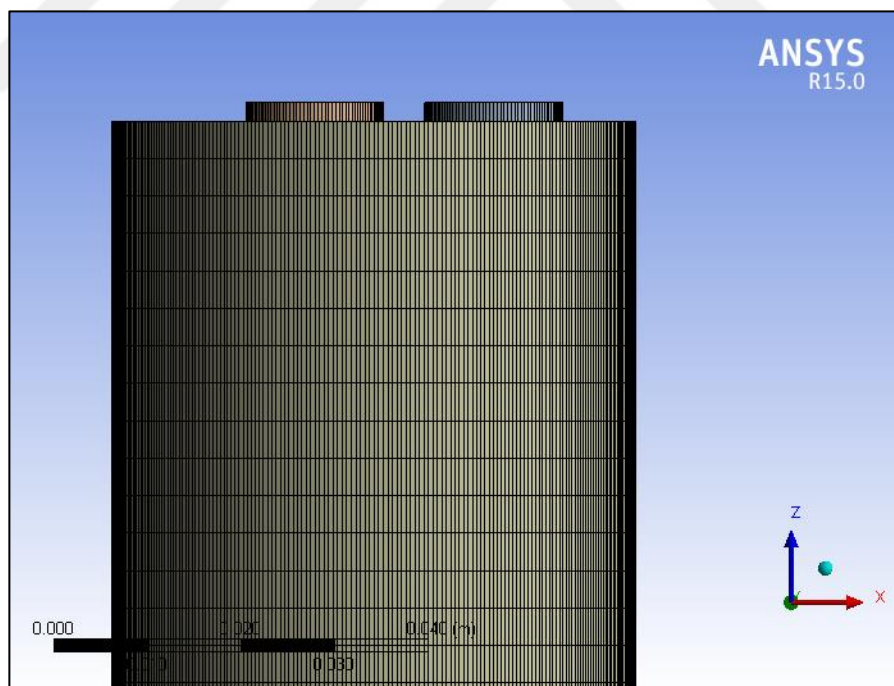46

Figure 3.13: Model with final mesh for triple model.

Figure 3.14: Mesh section of the receiver tube along the z-axis for the triple model.

47

3.6.2 Single Copper Tube Model

The number of cells has been increased until the results became stable. The temperature increases every one meter changes with the mesh cell number until it becomes stable at 4.6 million hexahedral cells, as shown in Figure 3.14. The z-axis is the length of the receiver tube, which has 500 divisions (Figure 3.15). In Zone 1, the perimeter of the glass tube has 180 divisions with established 6 nodes on the tube wall thickness. In Zone 2, the nanofluid area also has 180 divisions and 26 established nodes in the depth of the nanofluid towards the z-axis. In Zone 3, the perimeter of the copper tube has 180 divisions with 7 established nodes on the tube thickness. In Zone 4, the water area was likewise divided into 180 parts. Critical changes of temperature and velocity near to the walls needed a finer grid, especially in the water flow region. The cell size was 0.3 mm. All the divided parts have been made with each other in order to avoid any divergence in the solution. Figures 3.15 and 3.16 show every detail of the mesh.
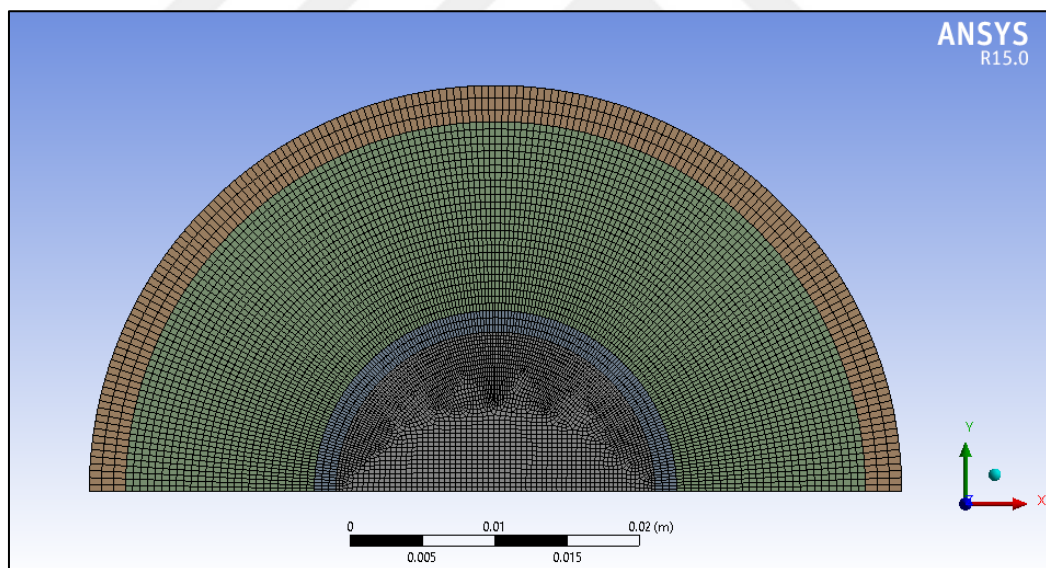
Figure 3.15: Single model with final mesh.
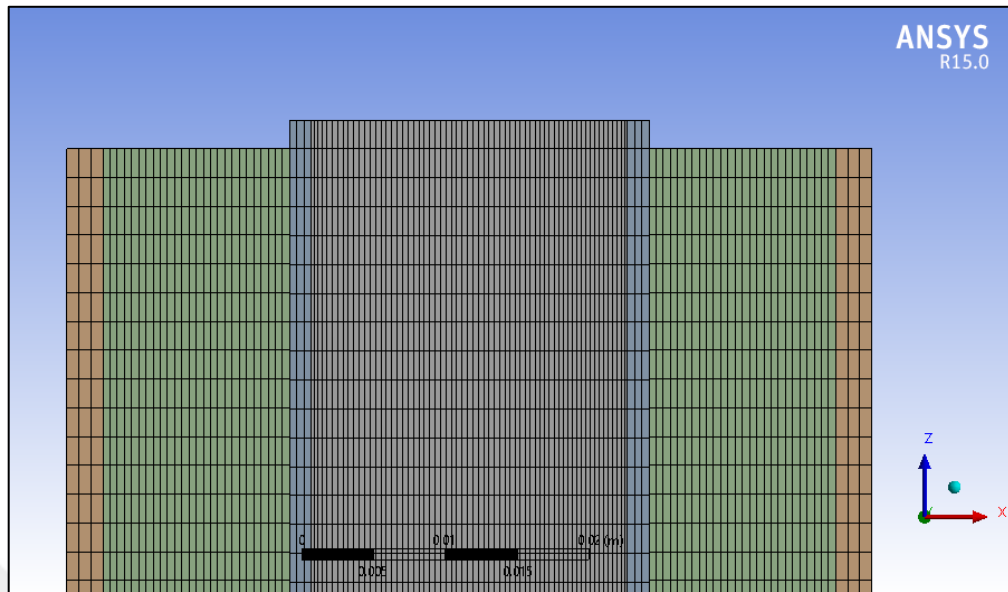
Figure 3.16: Mesh section of the tube along the z-axis for the single model.

3.7 Boundary Condition

We prepared the model simulation, and made it ready for application in the ANSYS FLUENT environment. The conditions had to be specified, and for these conditions, we had to be certain with high precision to obtain the correct results. The boundary condition provided for the model had to include temperature, mass flow rate, the heat generated inside the nanofluid, and so on. Despite this, the system was designed with high flexibility. The water inlet inside the copper tube was defined as a mass flow rate and the outlet was defined as an outflow with various flow rates (20, 40, 60, 80 liters/hour), and with a variety of temperatures (300°K, 315°K, 330°K), as shown in Table 3.7. The heat generated in the nanofluid and the heat losses were defined as the UDF file as previously interpreted.

Table 3.7: Boundary conditions used in models simulation.

Inlet		Outlet	Heat generated	Wall
Mass flow rate (kg/s)	Temperature K	Mass flow rate (kg/s)	Source term	Heat losses
0.0055, 0.011, 0.0166, 0.022	300, 315, 330	0.0055, 0.011, 0.0166, 0.022	UDF file	UDF file

3.8 Experimental Setup

Many practical studies have been conducted in the field of concentrated solar energy in order to test these systems and to measure their efficiency and usability in different countries and under different conditions. This will be an important source of energy in the future. Moreover, the advantages enjoyed by this type of system will include environmental friendliness as it produces no polluting emissions, and it has lower long-term costs compared to traditional power plants.

3.8.1 Design and Manufacture of the Parabolic Trough Solar Collector

After the single copper tube model was chosen as the best in terms of efficiency, we adopted the theoretical design of the parabolic trough solar collector. The model was actually manufactured and consists of seven parts, as follows:

3.8.1.1 The Iron Structures

The main function of this structure is to carry the reflector plate, receiver tube, and the control rod at the angle of the reflector, as shown in Figure 3.17. The structure was created with dimensions 1.05 m width × 1.02 m length. The pipes were used made from iron strips with a square section. The structure is light weight and solid so as to facilitate installation and assembly in a desired location. It has been fitted with mounting bolts and a control rod to control the tilt angle of the reflector. The angle control mechanism is made with a serrated rod and is fixed with bolts to enable the user to change and select the angle.
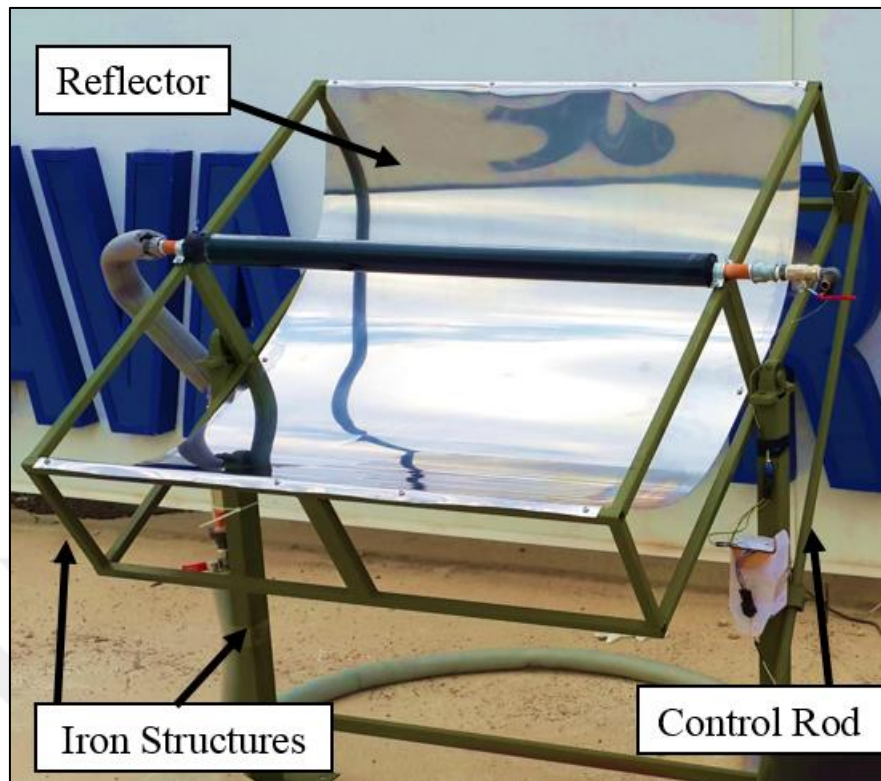
Figure 3.171: Solar Collector System.

3.8.1.2 Solar reflector

The solar reflector is a plate of stainless steel mirror prepared to give an appropriate focal distance (Figure 3.17). It is manufactured using special rolling devices and it is identical to the design dimensions of the plate in order to ensure the reflection of the solar radiation onto the focal line. The plate is fixed on an iron structure to obtain a coherent position that stays constant during motion because, if there is any small change during the test, it will influence the amount of reflected radiation onto the focal line. The manual tracking mechanism works with a serrated rod fixed by bolts, on which the soft teeth were selected to allow for precise control and to maintain the concentration of solar radiation on the focal line during the period of testing in order to obtain accurate results. The solar collector traced the Sun's motion from east to west.

3.8.1.3 Tubes

Two types of tube were used, namely the copper tube and glass tube, both of which were part of the absorber tube, an important part of the system. The copper tube extends horizontally at a length of 1.16 m and has an outer diameter of 25 mm. The tube extends along the focal line of the collector, where it is composited with the joints on the structure and fixed by screws with nuts, as shown in Figure 3.17. Thermocouples are installed at the inlet area and outlet area with specific tools. The glass tube has a length of 1 m and the nanofluid fills the cavity between the copper tube and glass tube.

3.8.1.4 Flow Meter

A flow meter is a tool used to measure the flow rate of the fluid moving into the receiver tube. It has a gradient of 10-100 liters/hour as (Figure 3.18). It was installed before the fluid inlet. The accuracy of the instrument was checked by checking the flow rate of less than 20 liters/hour with the required time. The experimental investigation was performed for four entry flows from 20 liters/hour to 80 liters/hour.

Figure 3.18: Flow meter.

3.8.1.5 Control Valve

After the flow meter was installed in the place before entering the liquid, a control valve was installed at the entrance point of the liquid to ensure that the liquid would not return. Another valve was installed at the liquid exit point to obtain complete and precise control, which in turn led to accurate results. Both control valves have a diameter of 12 mm (Figures 3.19 and 3.20).

Figure 3.19: Check valve at the liquid inlet.

Figure 3.20: Ball type valve at the liquid outlet.

3.8.1.6 The Pump

The function of the pump is to pump the water into the absorber tube and in different flow amounts up to 100 liters/hour. The pump is installed to convey the water from the tank to the absorber tube. The water pump used here has a flow rate of 30 liters/minute.

3.8.1.7 Digital Thermometer and Thermocouples

The thermometer function is the measurement of water temperature when entering and exiting the absorber tube, as shown in Figure 3.21. A type K thermocouple was used in this experimental work, as shown in Figure 3.22. Wires were connected between the thermocouple and the digital thermometer, which reads and records the data.

Figure 3.21: Digital thermometer.

Figure 3.22: Thermocouple type K.

3.8.2 Preparing the Nanofluid

Nanofluids are a new category of fluids engineered by dispersing nanoparticles (nanometer-sized materials) in base fluids., There are two methods to prepare a nanofluid. The first is called the one-step method, and the second is called the two-step method. The two-step method is broadly applied to prepare the nanofluid. In this study, the two-step method has been used as it is a less expensive method to prepare a nanofluid and it can be used on a large scale. The CuO nanofluid was prepared according to the second method. Initially, the CuO nanoparticles were weighed in grams to prepare a volume concentration of 0.075% using Eq. (3.27). The weight of the nanoparticles was 5.62 grams for one liter of nanofluid so as to prepare 0.075% concentration. Then the nanoparticles are mixed with the base fluid by mixing it over two hours in a blender. This was repeated two times to prepare two liters. The nanofluid was prepared by the Nanografi Company in Ankara.

3.8.3 Solar Radiation Intensity Computation

Solar radiation measurement is one of the important factors in our study, where the intensity of solar radiation was assumed to be $400 \, \text{W/m}^2$ in the simulation. The application of the Smartphone Okapi solar calculator by GREENHILL ENVIRO TECHNOLOGIES INC, was used to measure radiation intensity in this study. After calibrating the smartphone, we measured the solar radiation with the application, the measurements of which appear in Figure 3.18.
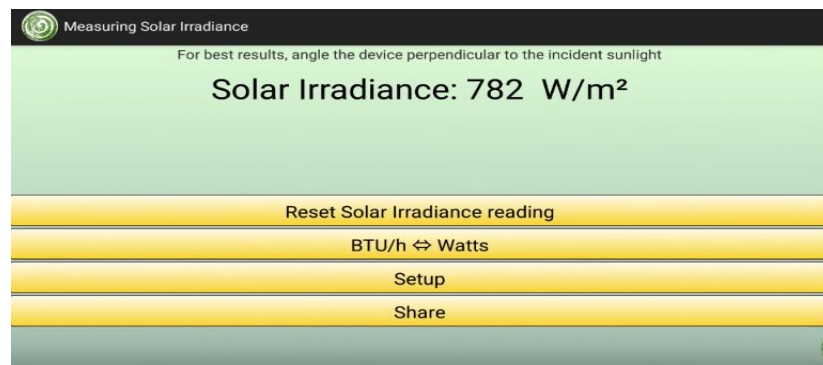

Figure 3.23: Application interface for measuring solar irradiance [57].

3.8.4 Computing Thermal Efficiency

The measurement and check of the thermal efficiency rely on the increase in temperature difference between the inlet and outlet temperatures of the tube and the direct solar radiation (G), which is measured at the same time as the difference in temperature. In such PTSC designs, the tests usually proceed for 10 minutes and for every record of the reading. Thus, the data recording was 500 readings. By these readings, one can calculate the thermal efficiency as follows [48]:

$$\eta_{th} = \frac{\dot{m}\, C_p \left(T_{wo} - T_{wi}\right)}{G.A_a} \tag{3.40}$$

CHAPTER FOUR
RESULTS AND DISCUSSIONS

4.1 Introduction

In this chapter, both experimental and numerical results are calculated to estimate the performance and efficiency of the new design model of the parabolic trough solar collector with direct absorption. Both the experimental and numerical results will be discussed. Firstly, the numerical results were obtained by utilizing the ANSYS FLUENT software, where it was utilized to solve the theoretical equations for two models of a direct absorption parabolic trough solar collector and to select the optimal model in order to adopt it in the study. Secondly, we built the selected model to conduct the study in practice. The experimental results which were obtained by building the model are compared with the theoretical results.

4.2 The Optimal Model

The simulation has been performed for two different models and the use of temperature calculation equations and efficiency, to choose the better of the two models in terms of efficiency and performance. The first model contains a single copper tube expanding inside the glass tube. The second model contains three copper tubes expanding inside the glass tube. The three copper tubes have the same volumetric capacity as the single copper tube in the first model. The purpose of determining the optimal model is to create an experimental model and comparison of experimental results with numerical results. Figure 4.1 shows the thermal efficiency for the two models with different volumetric flow rates (liters/hour) and the impact of changing the design of the copper tube with a fixed glass tube size. The results were found for the two models after being examined.

The efficiency of the collector with the triple tubes was lower as the presence of the three tubes in this configuration makes narrow passages for the movement of hot and cold nanofluid, as shown in Figures 4.2 and 4.3. The spaces between the three tubes and the space between the upper two tubes and glass tube were not sufficient for the free circulation of nanofluid. The hot nanofluid would accumulate on the left and right side which faced obstructions to rotate around the upper cold tubes. Therefore,

the maximum temperature of the nanofluid increased significantly to approximately 340°K. In Figure 4.2, the velocity vectors of the nanofluid show the following: the interaction between the boundary layers around the two upper copper tubes gave considerable flow resistance at distances between the two tubes, and the large thickness of the thermal boundary layer (Figure 4.2) and the large thickness of the momentum boundary layer (Figure 4.3) caused decreased heat transfer from the side of the lower tube.
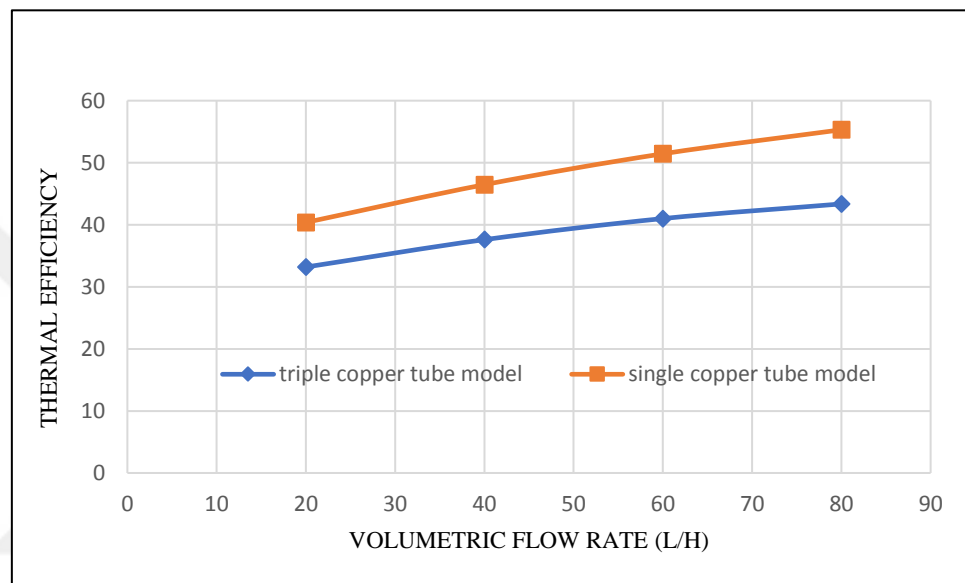

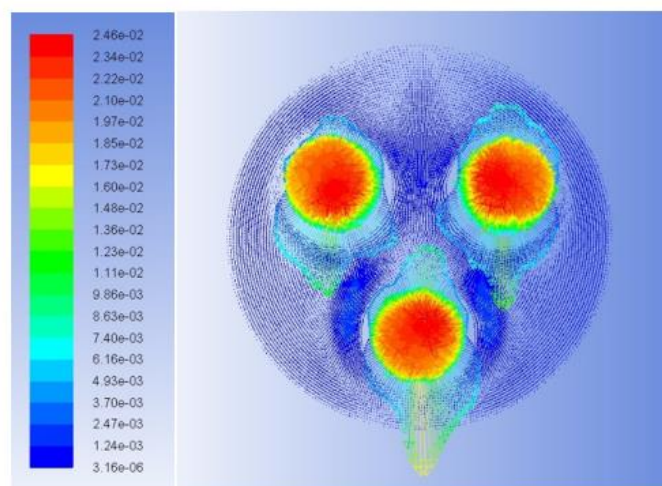**Figure 4.1:** Thermal efficiency for the two models with differences of volumetric flow rate (liters/hour).

Figure 4.2: Velocity vectors for the nanofluid and water zones in the triple copper tubes.
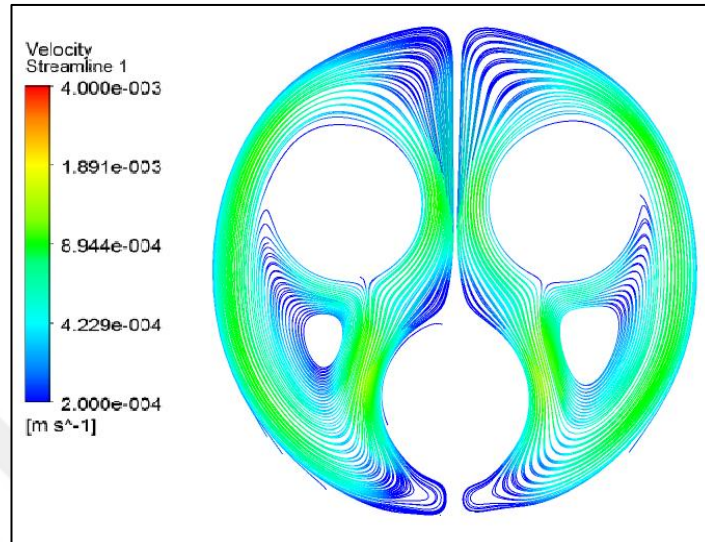
Figure 4.3: Velocity streamline for nanofluid and water zones in triple copper tubes.

In the single copper tube models, as shown in Figures 4.4 and 4.5, the temperature distribution around the copper tube is regular. Moreover, the streamline velocity and velocity vectors near the copper tube wall are greater than the streamline velocity near to the glass wall. As the velocity is higher closer to the copper tube wall than it is to the wall of the glass tube, the heat exchange between the nanofluid and the copper tube is higher from the heat exchange between the nanofluid and the glass tube wall. This will lead to reducing the heat losses, due to the heat exchange being a low between the nanofluid and the glass wall. This will result in increasing the efficiency and performance of the solar collector.

Therefore, the single copper tube model is the best model to convey heat between the nanofluid and water flow inside the copper tube. Here, efficiency reaches 55.31% for the single model, while it is 43.36% for the triple model.
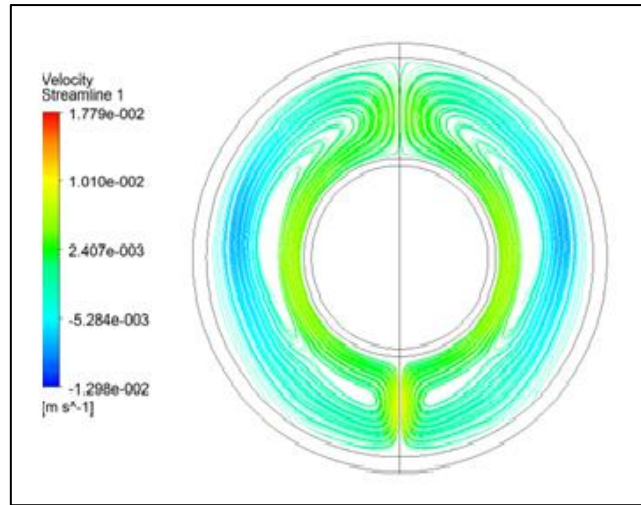
Figure 4.4: Velocity streamline for nanofluid and water zones of the single copper tube.
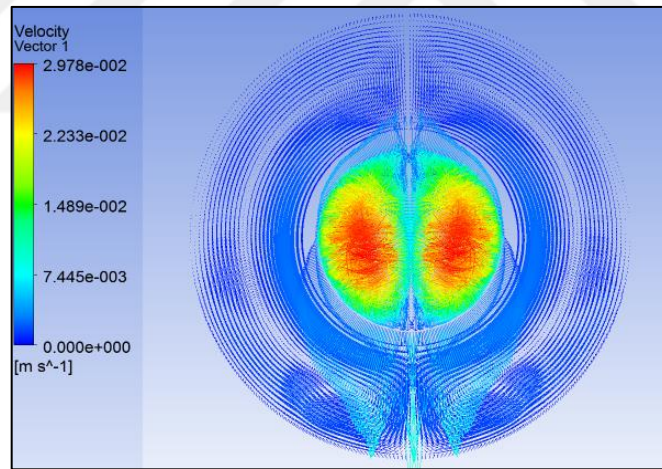
Figure 4.5: Velocity vectors for nanofluid and water zones for single copper tubes.

4.3 Numerical Results

The theoretical study was carried with the ANSYS FLUENT software to simulate the desired model. Both the heat generated and the thermal losses were calculated with the UDF (User-Defined Function) for each and applied in ANSYS FLUENT. The UDF codes were written in C language. The heat profile generated within the nanofluid was used as a source term. The theoretical calculations were

performed according to boundary condition and the engineering design of the model. The modeling was done for 24 cases, which were different in terms of design, inlet temperatures, and different concentration ratios of nanofluids. The results obtained from this calculation found that the performance efficiency of the model ranged from 40.38% to 55.31%, with a varying volumetric flow rate from 20 to 80 liters/hour as shown in Table 4.1. The equation of thermal efficiency is as follows:

$$\eta = \frac{\dot{m} \, Cp \, \Delta T}{A \, G} * 100\%$$

where ΔT is the difference value between the inlet and outlet temperatures of the water, Cp the specific heat capacity, $\dot{m}$ the mass flow rate, G the solar radiation of 400 W/m^2, and A the surface area of the glass tube.

Table 4.1: Numerical results by ANSYS program simulation.

Mass flow rate of water l/h	Inlet temperature of water (K)	Outlet temperature of water (K)	ΔT (K)	η %
20	300	307.3	7.3	40.38
40	300	304.2	4.2	46.46
60	300	303.1	3.1	51.44
80	300	302.5	2.5	55.31

4.3.1 Performing Refinement of the Mesh

The convergence study needs the choice of a convenient scale in order to purify the grids. This scale may be either local or global. This will allow for the definition of the scale in one location on the form or as an integral part of the fields on the whole model area, which will lead to a change in the purity of the mesh, and the solution still not completing a mesh-independent solution. The mesh needs more refinement and iterates the process until the solution is independent of the mesh. It is necessary to utilize the smallest mesh to decrease the simulation run time and provide a mesh for an independent solution. We used the efficiency as a variable parameter to study the change of the mesh on it with an increasing mesh number. In the single tube model,

beginning with 600000 cells and increasing the number of meshes ten times, every time increasing by 500,000 cells, the efficiency increasing by 600,000 cells was 43%; then it increased to 55.3% and settled at 4,600,000 cells. In the triple tube model, the same previous procedure was performed and the efficiency increasing to 600,000 cells was 30.7%; then it increased to 43.36% and settled at 5,300,000 cells.

When increasing the mesh number, we observed an increase in the value of the efficiency to 55.3% at a 4,600,000 mesh number in the single tube model. At a 5,300,000 mesh number, the efficiency reached 43.36% in the triple tube model, as shown in Figure 4.6. By growing the mesh numbers further, we found that for a 5.6 million mesh number, the value of the simulation results was within an agreeable range. This refers to achieving a solution value which is independent of the mesh solution, where it can use the 4,600,000 mesh number for the single tube model, and the 5,300,000 mesh number for the triple tube model, which will provide results within the user disparity.

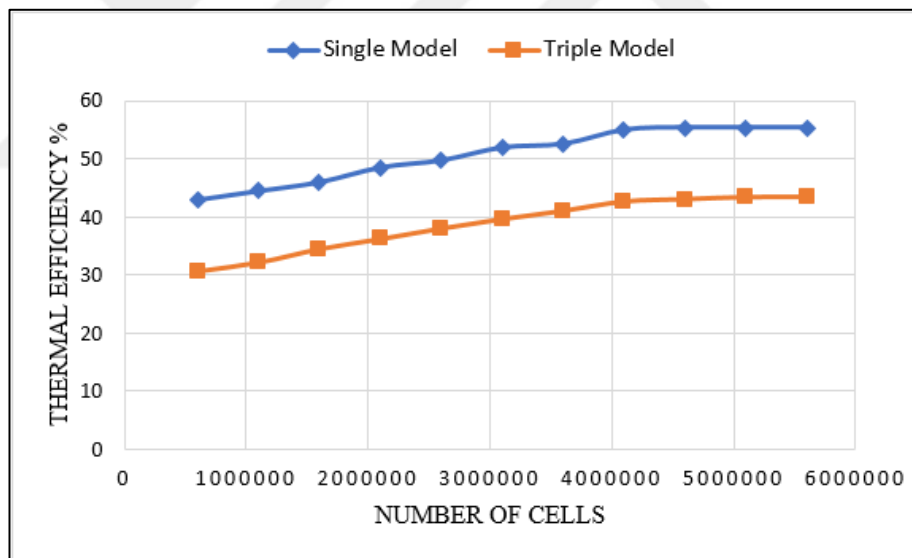**Figure 4.6:** Mesh refinement by increasing the mesh number with a rise in efficiency.

4.4 Experimental Results

The experiment was performed in which the temperature was examined at four different flow rates (20, 40, 60 and 80 liters/hour) for the entry and exit of the water, thereby calculating the efficiency. The temperatures were measured with the thermometer device, which was previously indicated in this study, according to

ASHRAE Standard [RA91] 93-1986 [58]. The value of the ambient temperature was 27°C and for the solar radiation, it was 400 W/m^2.

4.5 Experimental Results in Comparison to Theoretical Results and Discussion

The purpose of comparing the experimental and theoretical results is to prove and confirm the validity of the results obtained from the simulation. Table 4.2 shows the theoretical and experimental results and the percentages of error between them. The error rates ranged from 3.17% to 5.6% according to the different flow rates. Moreover, the percentage was within the permissible range. Figure 4.7 shows the change in temperature gradient with a different flow rate for both the numerical and experimental results. Figure 4.8 shows the thermal efficiency of the collector at a different volumetric flow rate for each of numerical and experimental result. The results presented growing thermal efficiency when increasing the flow rate of the water. This matches with the experimental results in Figure 4.8.

Table 4.2: Numerical and experimental results with error percentages.

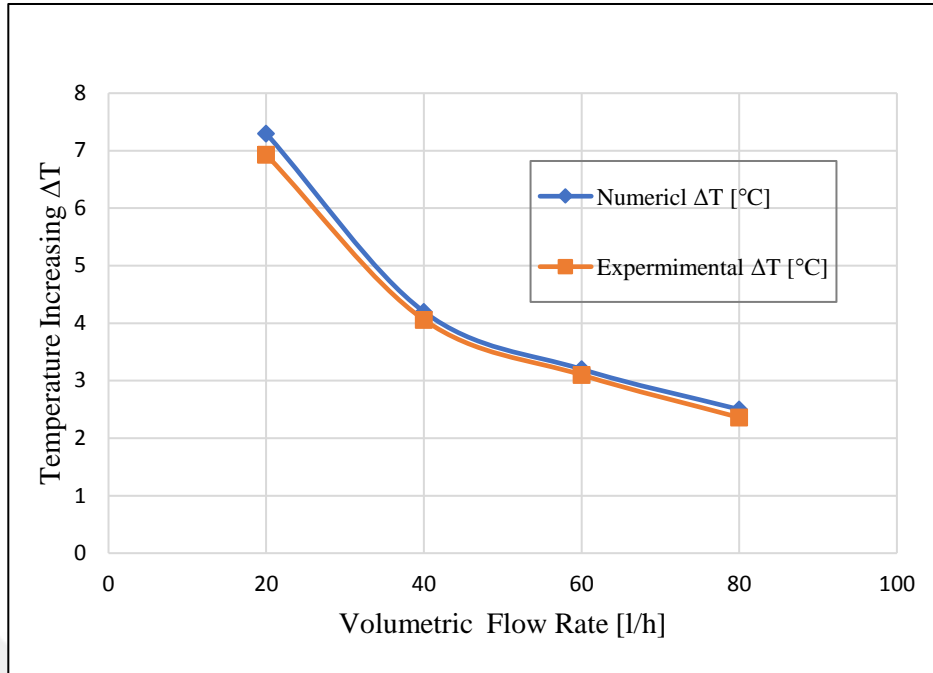| Volumetric Flow rate [l/h]	Numerical results ΔT [°C]	Experimental results ΔT [°C]	Error%
20	7.3	6.93	5.02
40	4.2	4.06	3.17
60	3.1	3	3.22
80	2.5	2.36	5.6

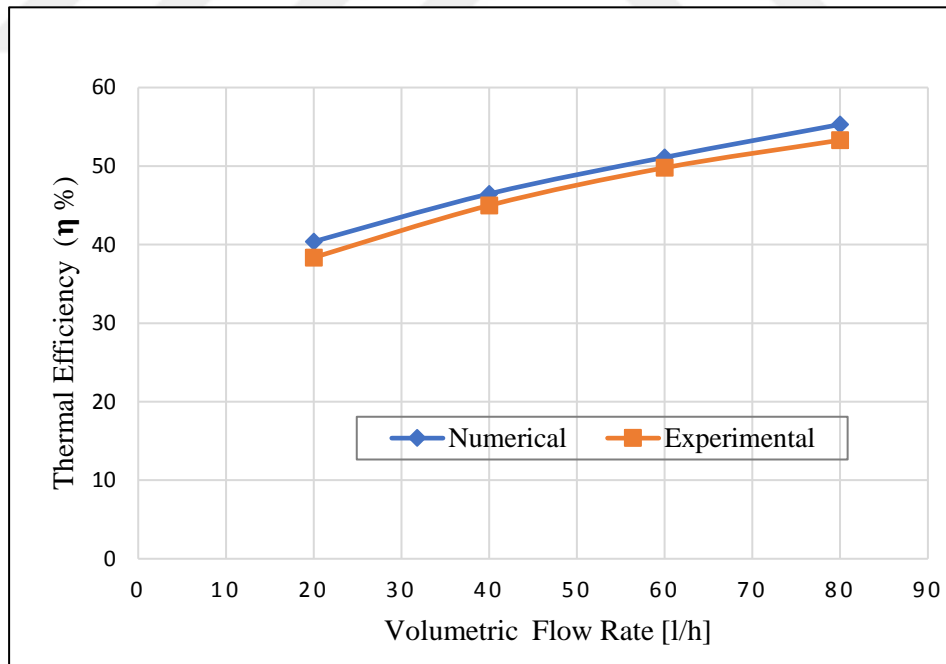**Figure 4.7:** Increasing the temperature with different flow rates for numerical and experimental results.

Figure 4.8: Numerical and experimental results of thermal efficiency with different volume flow rates.

4.6 Effect of Inlet Temperature on Water

4.6.1 Effect of Inlet Water Temperature on Outlet Water Temperature

After the theoretical calculations were verified and their results matched with the experimental results, other simulations were performed under the same conditions and assumptions. However, the inlet temperature of the water was changed as follows: 300°K, 315°K and 330°K, at the same previous flow rates (20, 40, 60 and 80 liters/hour). The results showed that increasing the temperature of entry to the liquid led to a reduction of the temperature of the exit and this was due to increased thermal losses. Figure 4.9 shows the decrease in temperature.
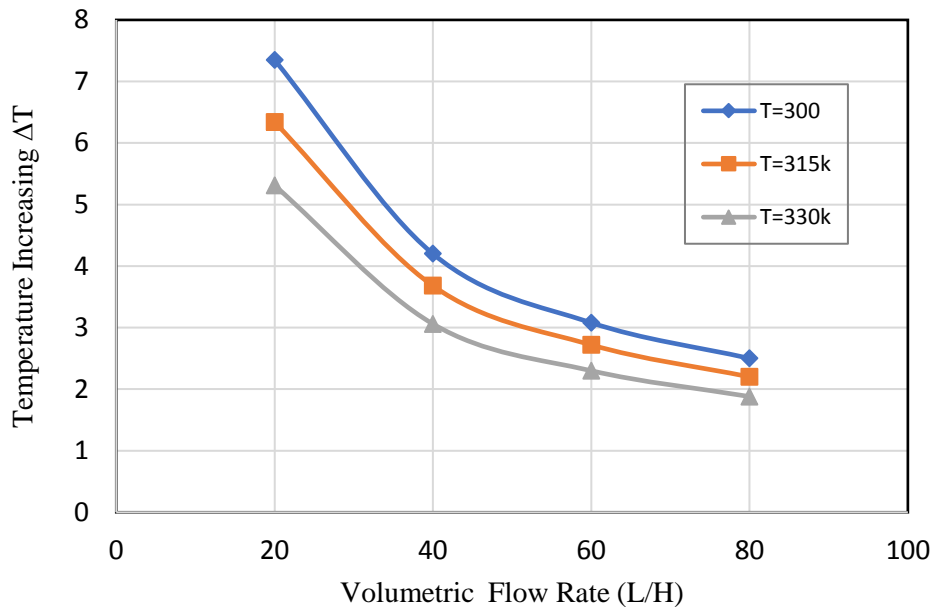

Figure 4.9: Various inlet temperatures at several volumetric flow rates.

4.6.2 Effect of Inlet Water Temperature on Thermal Efficiency

The figure below shows that thermal efficiency increases with an increase in the flow rate. An increase in the inlet temperature leads to a decrease in the thermal efficiency. The explanation for this is that thermal efficiency depends on the amount of heat gained by solar radiation. This heat gained depends on the inlet temperature, which decreases as the temperature of the inlet increases. Figure 4.10 shows the blue curve representing a change in thermal efficiency at an inlet temperature of 300°K and

65

the orange curve shows the change in thermal efficiency at an inlet temperature of 315°K. The yellow curve shows the change in thermal efficiency at an inlet temperature of 330°K.
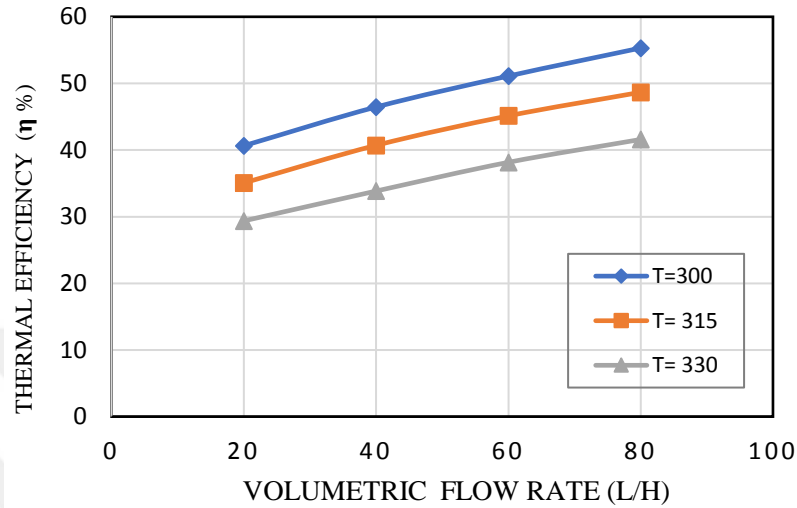

Figure 4.10: Change of thermal efficiency with the inlet temperature of water.

4.6.3 The Effect of Different Inlet Temperatures of Water in Nanofluid Temperatures with Different Mass Flow Rates.

Figures 4.11 and 4.12 show the heat distributions in the nanofluid zone and the water flowing through the copper tube, where the temperature of the inlet water was 300°K and for the two various cases of flow rate, namely 40 and 80 liters/hour. It was noticed that when the flow rate increased, the water temperature rose as the flow rate increased. Moreover, there was a uniform gradual rise in the nanofluid temperature.

Figure 4.11: Heat distribution for different cross sections at 300°k inlet temperature at a flow rate of 40 liters/hour.

66

Figure 4.12: Heat distribution for different cross-sections at 300°k inlet temperature at a flow rate of 80 liters/hour.

In Figures 4.13 and 4.14 with same previous section at a 315°K inlet temperature of water, it was observed that both the water and nanofluid temperatures gradually increased with the flow rate.

Figure 4.13: Heat distribution for different cross-sections at 315°k inlet temperature at a flow rate of 40 liters/hour.
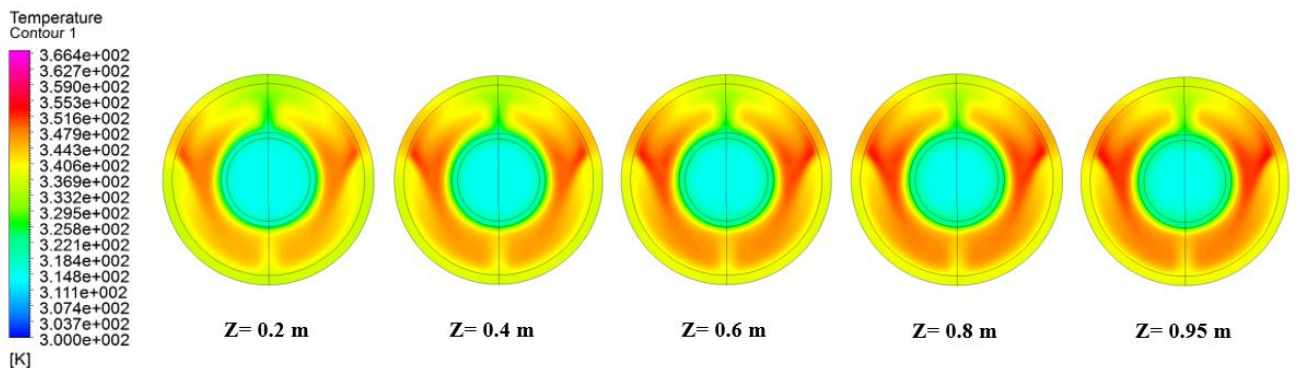
Figure 4.14: Heat distribution for different cross-sections at 315°k inlet temperature at a flow rate 80 liters/hour.

In Figures 4.15 and 4.16, also with the same previous section at 330°K inlet temperature of water, it was noted that there was a large increase in both the water temperature and nanofluid temperature, but the change in water temperature with the flow rate was very small due to the gain being low.
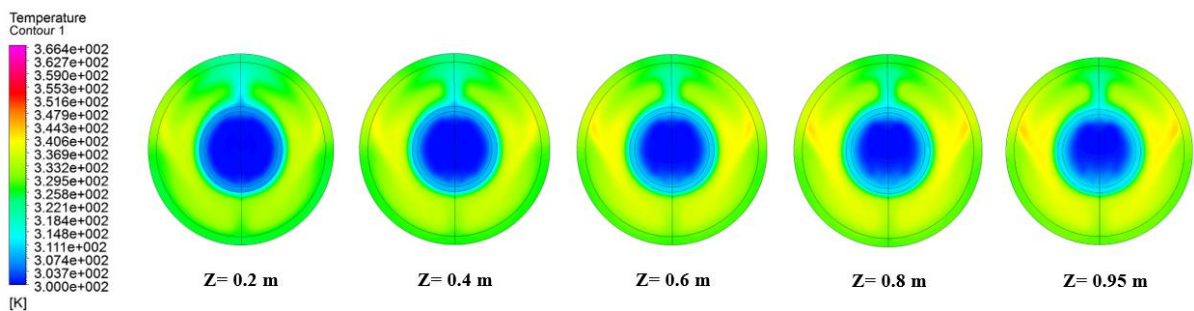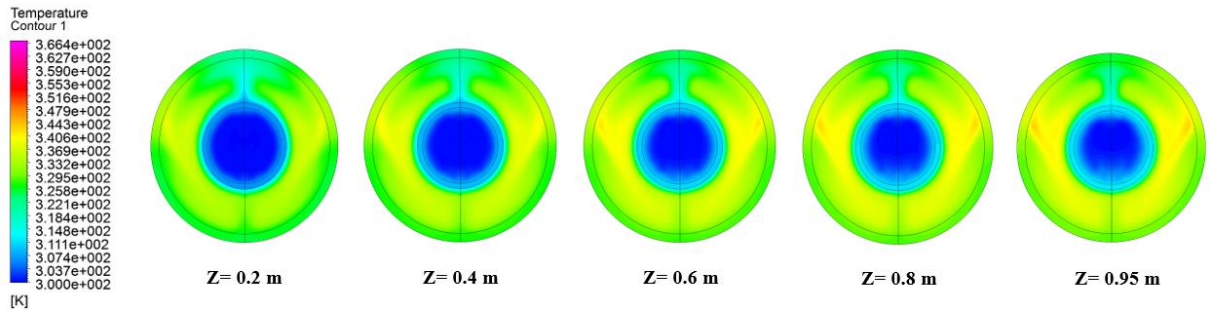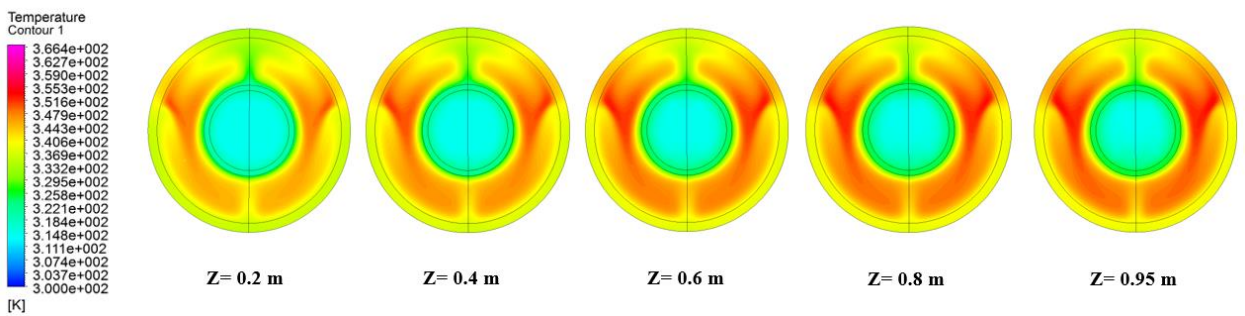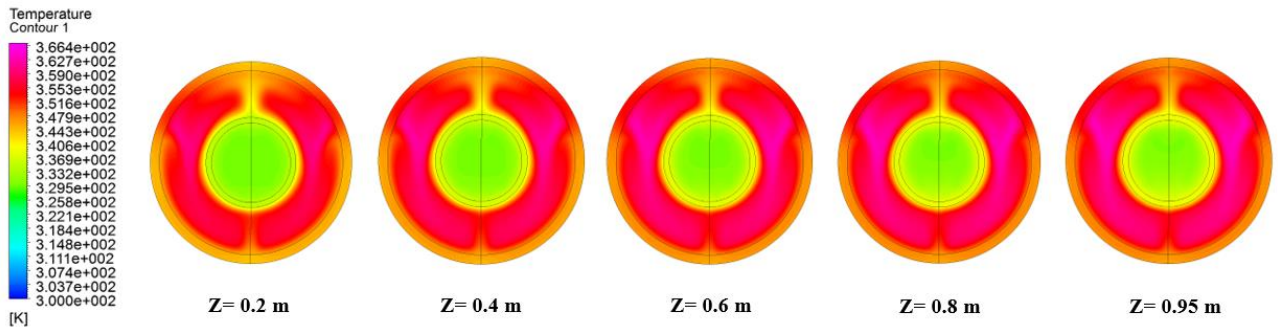

Figure 4.15: Heat distribution for different cross-sections at 330°k inlet temperature with a flow rate of 40 liters/hour.
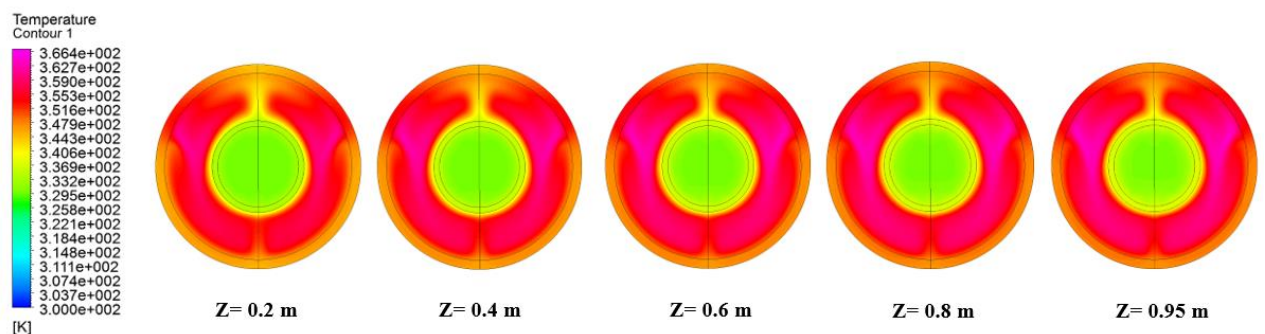
Figure 4.16: Heat distribution for different cross-sections at 330°K inlet temperature at a flow rate of 80 liters/hour.

4.7. Profiles of the Temperature Distribution for the Nanofluid Zone along the Absorber Tube

Figure 4.17 shows the profiles of the temperature distribution in the nanofluid zone, where the nanofluid absorbs the direct solar radiation. The figure shows the thermal gaps along the tube and the heat exchange between the nanofluid and the water flowing inside the copper tube, and how the gaps differ from one area to another along the tube.
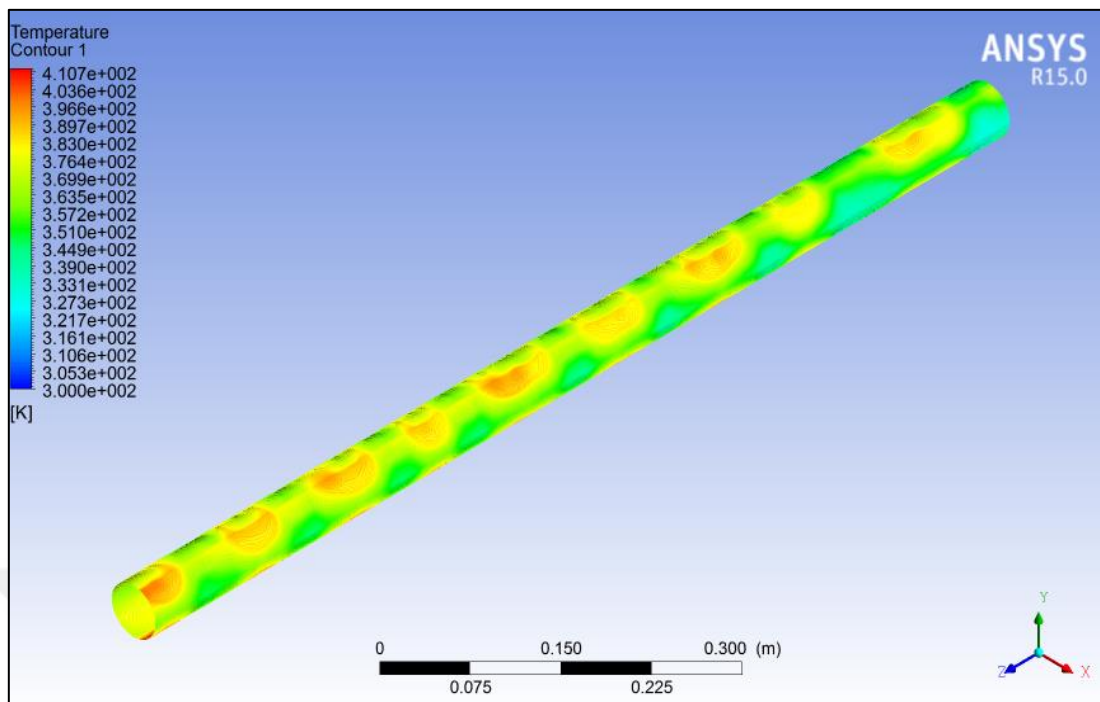
Figure 4.17: Temperature distribution profiles of the nanofluid zone.

4.8 Profiles of the Temperature Distribution for the Water Zone along the Absorber Tube

Figure 4.18 shows the temperature volume rendering of water, where the temperature gradient appears in the water region showing the increase in temperature in the water layers close to the wall of the copper tube. Figure 4.19 shows the increase of water temperature through its flow along the tube.
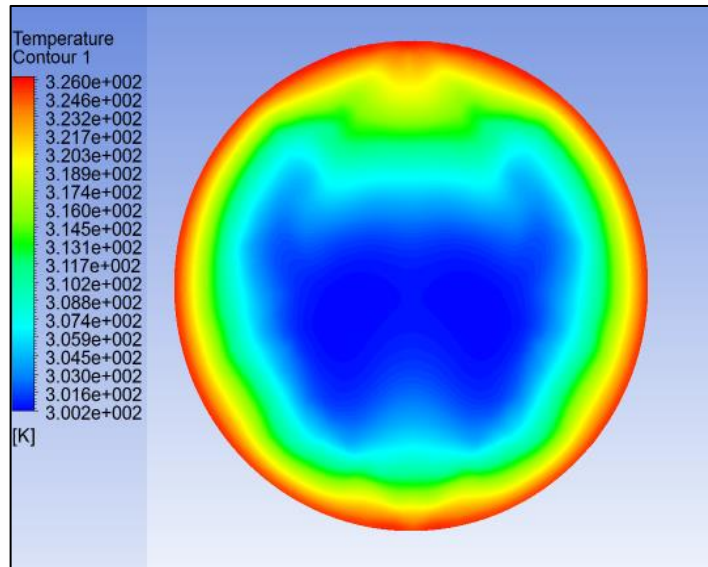
Figure 4.18: Cross section of the temperature distribution of the water.
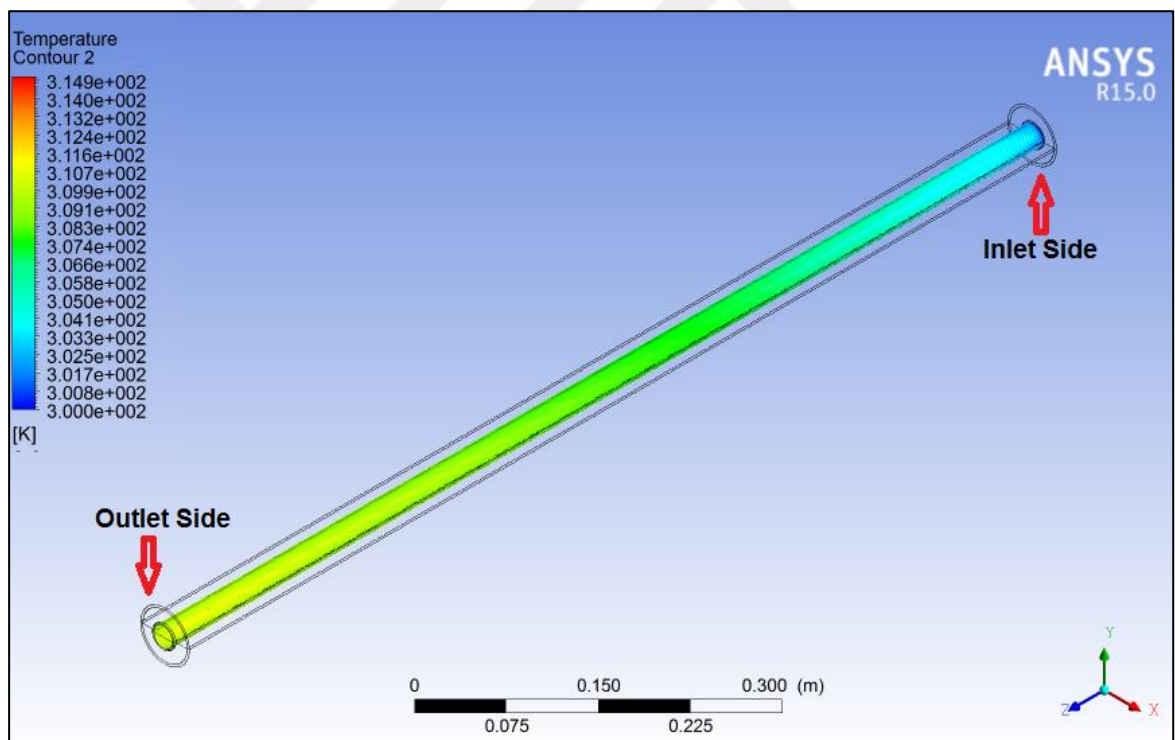
Figure 4.19: Profiles of the temperature distribution for the water zone.

4.9 Profiles of the Velocity Streamline in the Nanofluid Zone

Figure 4.20 shows the velocity streamline. As a result of the heat exchange between the nanofluid and the water flowing through the copper tube, and due to the nanofluid being non-circulating and the difference between the temperatures of the nanofluid and water, this will cause a natural convection process. Figure 4.20 shows the velocity streamline caused by the natural heat convection in the nanofluid zone.
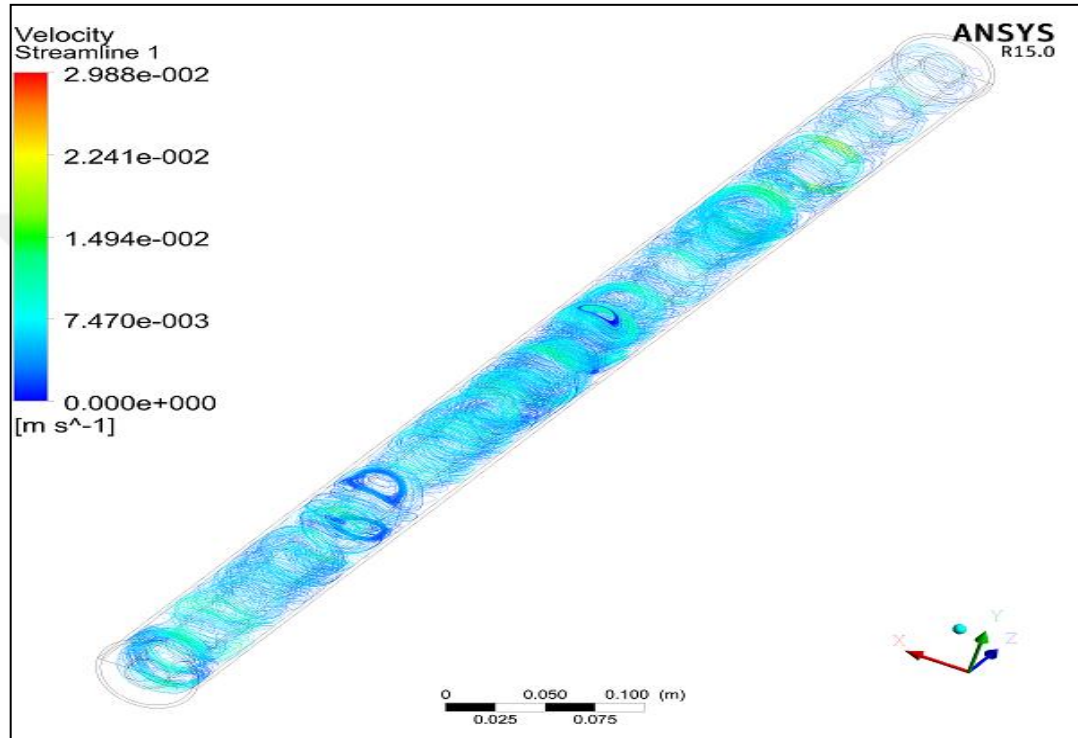
Figure 4.20: Profiles of the velocity streamline of the nanofluid zone.

4.10 Effect of Volume Flow Rate on Thermal Efficiency

Figure 4.21 shows the increase of thermal efficiency when the volumetric flow rate increases. The increase in the volumetric flow rate will cause a rise of the Reynolds' number, which results in increasing the heat exchange between the nanofluid and the water flowing inside the copper tube. An increase of efficiency was noticed with an increase in the Reynolds numbers. In spite of the flow being assumed to be laminar flow in this study, the flow remained laminar in all cases.
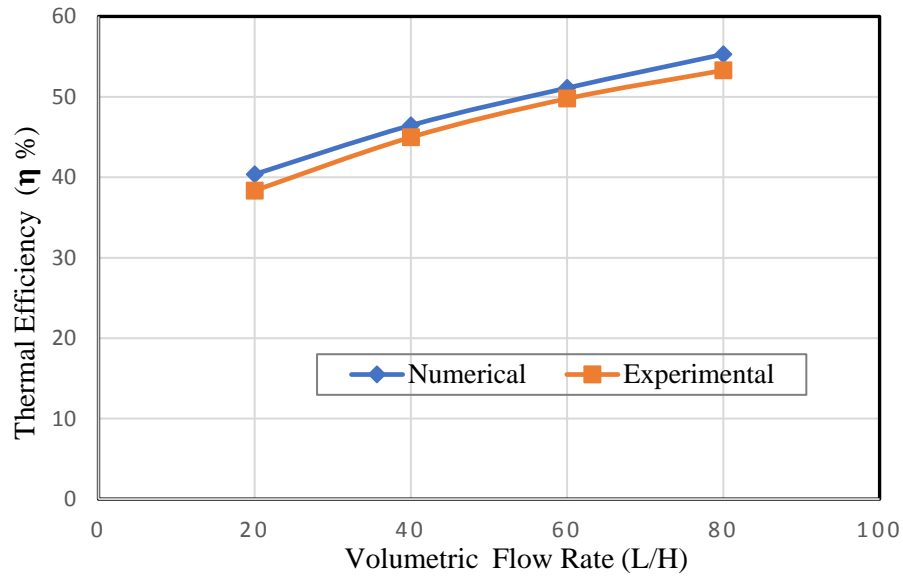
Figure 4.21: Thermal efficiency changing with different volumetric flow rates.

4.11 Effect of Various Volume Fraction of Nanofluid

4.11.1 Effect of Various Volume Fraction of Nanofluid on Absorption Solar Irradiance

The solar energy absorbed by the nanofluid represents an internal heat source as explained previously by Eq. (3.8). The use of an internal thermal source explains the movement of solar radiation within the nanofluid. Moreover, the radiated beam changes with the outer perimeter of the tube resulting from the different angle of the reflection of the radiation towards the tube. This causes a change in the internal heat source. As shown in Figure 4.22, the differences in the optical depths for the three different heat sources in the concentration ratio are 0% (only synthetic oil without nanoparticles), 0.05% and 0.075%. At the concentration of 0% (without nanoparticles and only synthetic oil), it was found that the absorption radiation was very small and almost non-existent because the absorption coefficient of the oil without nanoparticles is very low. At a concentration of 0.05%, it was observed that the absorption of radiation was along the optical depth, while at 0.075% concentration, it was observed that the absorption was initially very high and started to decrease along the depth whenever it goes inside the nanofluid. Moreover, it was observed that there was no solar radiation in the lower area of the tube due to the shadow of the tube.

72
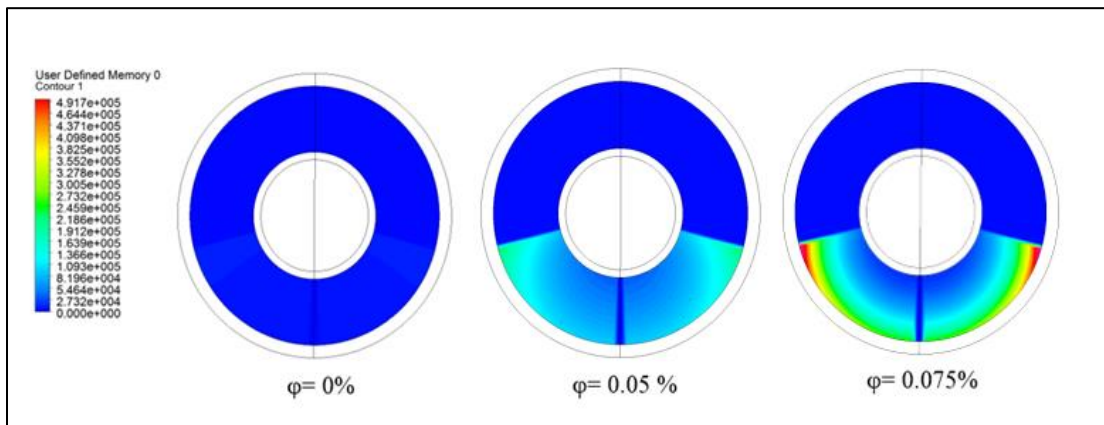
Figure 4.22: Three different internal heat sources with optical depth for three different concentrations (0%, 0.05% and 0.075%) of nanofluid.

4.11.2 Influence of the Volume Fraction Ratio of Nanofluid on Thermal Efficiency

Figure 4.23 shows the change in thermal efficiency in a volume fraction of nanofluids. It was observed that the thermal efficiency increases when increasing the volume fraction of nanofluids. The efficiency reaches 55.31% at 0.075% concentration while the efficiency is 43.36% at 0.05% concentration and 2.2% at 0% concentration with only synthetic oil.
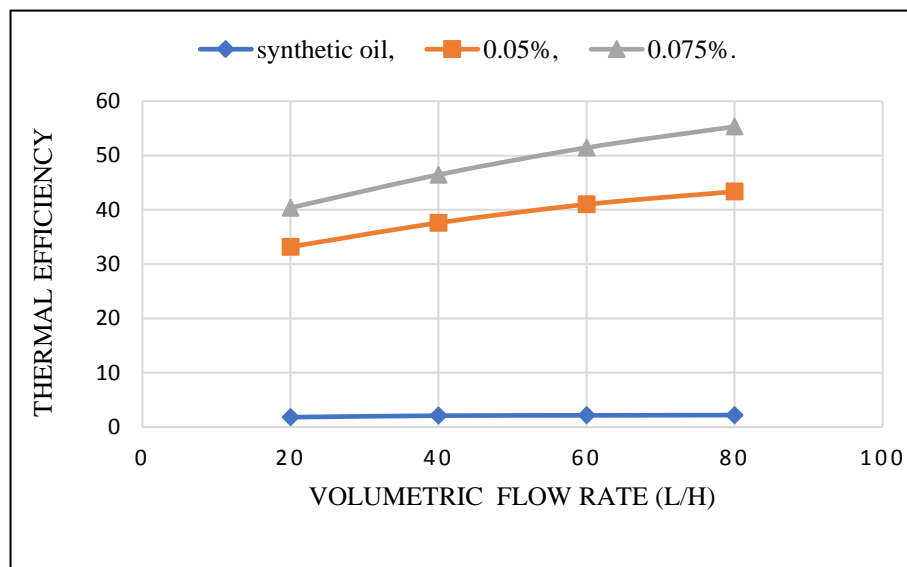
Figure 4.23: Influence of the volume fraction ratio on thermal efficiency.

4.12 Cost of the Model

The cost of the new model used in this study is considered to be low compared to the traditional model. The cost of the new model is $450 while the cost of the traditional model is $1000. This is due to the design of the new model, where two pumps are used in the conventional model, one for the nanofluid and the second for the liquid to be heated, while in the new model, only one pump is used because the nanofluid is uncirculated and therefore does not require a pump. In addition to the cost of the nanofluid, the conventional model needs a larger amount of nanofluid, while the new type needs less nanofluid. Another advantage of the new model is that it takes less space than the conventional model due to it being smaller, with the conventional model having the external heat exchanger. In the new model, the heat exchanger is integrated into the absorber tube as one component. This, in turn, reduces the amount of thermal resistance and as a result, the performance and efficiency of the system is higher.

CHAPTER FIVE
CONCLUSIONS AND FUTURE WORK

5.1 Conclusion

The main objective of this research was to improve the efficiency of the direct absorption solar collector for solar energy harvesting by improving the absorption of solar radiation by using a nanofluid in the collector. We used copper oxide nanoparticles with a synthetic oil as a nanofluid uncirculated in a one-meter length glass tube to absorb the concentrated solar radiation directly and convert it into heat energy which is then transferred to the water flowing into the copper tube extending inside the glass tube and being surrounded by the nanofluid. Both the glass and copper tubes will work as a direct heat exchanger.

First, the model has been numerically simulated and examined using the ANSYS FLUENT Software of the model according to the boundary conditions and characteristics identified in Chapter Three. Efficiency was calculated for the four flows at 20, 40, 60 and 80 liters/hour, and the efficiencies were 40.38%, 46.46%, 51.44% and 55.31%, respectively.

Second, experimental results were taken. After the experimental model was created, the value of the solar radiation was found to be 400 W/m^2 and the ambient temperature 27°C. The practical examination and recording of the readings were performed for four flows (20, 40, 60 and 80 liters/hour) and the efficiencies were found to be 38.35%, 45%, 49.78% and 52.36%, respectively.

Third, after the numerical and experimental results were obtained, they were compared, resulting in the percentages of error between them ranging from 3.17% to 5.6%.

The results showed that thermal efficiency increases with increasing volumetric flow rate, which is due to an increased heat exchange between the nanofluid and water; therefore, the heat losses from the wall to the atmosphere are lower. It also proved that efficiency is inversely proportional to the rising inlet temperature.

The results demonstrated that the use of synthetic oil without nanoparticles has very low or negligible efficiency, and an increase of the volume fraction of the nanofluid was directly proportional to the thermal efficiency, wherein the efficiency

was 34.07% at a volume fraction of 0.05%, while the efficiency was 55.31% at a volume fraction of 0.075%.

5.2 Future Works

The results of the study were encouraging and could be adopted and developed in future studies. Recommendations include the following:

• Utilizing different types of base fluid with a low-viscosity index.

• Adopting different sizes of the nanoparticle.

• Using different types and sizes for nanoparticle.

• Reducing thermal losses due to convection by utilizing an evacuated glass tube to cover the receiver tube, which will lead to a reduction of thermal losses and an increase in the efficiency of the solar collector.

• A model can be used as a base part of power plants, especially in countries with high amounts of solar radiation, such as Iraq and Libya.

Appendix (A)

A.1 UDF of Heat Generation

In order to create a UDF for the heat generated in a nanofluid which is produced by absorbing the solar radiation and in which the heat generated is a heat source, we define this source using a macro in order to define the equation mentioned previously to calculate the energy source and place the UDF as a source term in the nanofluid region. The UDF appears as below.

```c
#include "udf.h"

real abs_coeff = 214.0; /* absorption coefficient */
DEFINE_SOURCE(energy_source, cell, thread, dS, eqn)
{

real x[ND_ND];
real C;
real x1;
real y1;
real r;
real r000;
real source;
real rin = 0.0125;   /* radius inner tube*/

real rout = 0.0255;  /* radius outer tube*/

real n = 26;         /* number of division in annular */

real dr = (rout-rin)/n;
real PI=3.141592654;
real angle;
real Io; /* solar radiation intensity*/

C_CENTROID(x,cell, thread);
source = 0.0;
 x1=x[0];
 y1=x[1];
```

```
 r000 = sqrt(x1*x1+y1*y1);
 r = rout-r000 ;
angle = acos(x1/r000)*180/PI;
C= 10970/(1 + (x1/r000));
if (angle >= 2 && angle <= 75 )
{
Io = C*(1-(x1/r000))/(pow((y1/r000),2));
source = (Io*(1-exp(-214*(r+dr/2)))-Io*(1-exp(-214*(r-
dr/2))))/dr;
dS[eqn] =0.0;
}
else
{
source = 400;
}
C_UDMI(cell,thread,0)=source; /* This is UD memory*/


return source;


}
```

A.2 UDF of the Calculation of Heat Losses

A DEFINE_PROFILE macro has been utilized to compute the losses of the model with the free stream. Heat losses of the model change on every face in a cell due to the solar radiation being non-uniform around the absorber tube. The loss equation mentioned previously was used in the UDF. The losses in the UDF are as follows:

```
#include "udf.h"
DEFINE_PROFILE(UL, thread, position)
{
real  Tsky = 295;/*skay temperature*/
real v = 5 ; /* velocity of air */
real  ρ = 1.25; /* density of air*/
real u = 0.0000179; /* viscosity of air */
real εr = 0.88; /* emissivity of glass*/


real Ka = 0.0263; /*thermal conductivity of air */
```

78

```
real hw ; /*Heat transfer coefficient of air */
real Nu; /* nusselt number of air */
real Re; /* Reynolds number of air */
     real UL ; /* loss coefficient */
real Dr= 0.056; /* outer diameter of receiver tube */
real L = 1; /* length of tube */
real pi = 3.14;


real Ta = 300; /*ambient temperature of air */
real Ɛ = 5.67E-08 ; /* The Stefan-Boltzmann Constant */
real walltemp; /* wall temperature */
real Qloss; /*heat losses   */
cell_t c;
real x[ND_ND]; /* this will hold the position vector */
Nu=0.3*pow(Re,(3/5));
Re=(ρ*v*Do/u);
hw= Nu *(Ka/Do);
begin_c_loop(c,thread)
{
C_CENTROID(x, c, thread);
walltemp = C_T(c,thread) ; /* temperature of inner receiver tube */
Qloss= pi*Dr*L*hw*(walltemp-Ta)+εr*pi*Dr*L*e*(pow(walltemp,4)-
pow(Tsky,4));
C_PROFILE(c, thread, position) = Qloss/(pi*Dr*L*(walltemp-Ta));
}
end_c_loop(c, thread)
}
```

Appendix (B): Calculating Heat Convection

The value of heat convection is calculated in this section for the two simulated models. The temperatures of the nanofluid were obtained from the results of the ANSYS FLUENT software. The best model was chosen by calculating the efficiency of the two models. The single copper tube model was found to be the better model. In order to check the heat transfer for the two models, the heat convection was calculated, as follows:

The Properties from table (3.3) μ=0.07481 pa.s , k=0.1735 W.(m.K)$^{-1}$, Cp=1793 J.(kg.K)$^{-1}$,

   ρ= 1249.5 Kg.m^{-3}, β= 0.00064885 K^{-1}

momentum diffusivity $\nu = \dfrac{\mu}{\rho} = \dfrac{0.07481}{1249.5} = 5.9871*10^{-5}$ m^2/s

thermal diffusivity $\alpha = \dfrac{k}{(\rho.Cp)} = \dfrac{0.1753}{(1249.5*1793)} = 7.824*10^{-8}$ m^2/s

Prandtl's number $Pr = \dfrac{\nu}{\alpha} = \dfrac{5.9871*10^{-5}}{7.824*10^{-8}} = 765.22$

B.1 Single Tube Model

T_n= 345 K , T_w = 300 K

r_o= 0.0255 m , r_i = 0.0125 m

$$L_c = \frac{2\left[\ln\left(r_o / r_i\right)\right]^{4/3}}{\left(r_i^{-3/5} + r_o^{-3/5}\right)^{5/3}}$$

L_c= 2[ln(0.0255/0.0125)]$^{4/3}$ / (0.0125$^{-3/5}$ + 0.0255$^{-3/5}$)$^{5/3}$

L_c = 6.8973*10^{-3} m

$$R_{ac} = \frac{g.\beta\left(T_n - T_w\right)L_c^3}{\upsilon\alpha}$$

R_{ac}= 9.81*6.4885 x10^{-4} *(345-300)*(6.8973*10^{-3})^3/5.9871*10^{-5}*7.824*10^{-8}

R_{ac} = 20064

$$\frac{k_{eff}}{k} = 0.386\left(\frac{P_r}{0.861 + p_r}\right)^{1/4} Rc_a^{1/4}$$

k_{eff} = 0.386(0.1735)(765.22 /0.861+765.22)$^{1/4}$ *(20064)$^{1/4}$

$k_{eff} = 0.79$ W/m.K

$$q^- = \frac{2\pi.k_{eff}}{\ln(r_o / r_i)}(T_n - T_w)$$

$q^- = 2*\pi*(0.79)*(345\text{-}300)/(\ln(0.0255/0.0125))$

$q^- = 313.14$ W/m

B.2 Trible Tube Model

$T_n = 345$ K   , $T_w = 300$ K

$r_o = 0.0255$ m , $r_i = 0.00635$ m

$$L_c = \frac{2[\ln(r_o / r_i)]^{4/3}}{\left(r_i^{-3/5} + r_o^{-3/5}\right)^{5/3}}$$

$L_c = 2[\ln(0.0255/0.00635)]^{4/3} / (0.00635^{-3/5} + 0.0255^{-3/5})^{5/3}$

$L_c = 1.0802 *10^{-2}$ m

$$R_{ac} = \frac{g.\beta(T_n - T_w)L_c^3}{\upsilon\alpha}$$

$R_{ac} = 9.81*6.4885 \times 10^{-4} *(345\text{-}300)*(1.0802 *10^{-2})^3/5.9871*10^{-5}*7.824*10^{-8}$

$R_{ac} = 77071$

$$\frac{k_{eff}}{k} = 0.386\left(\frac{P_r}{0.861+ p_r}\right)^{1/4} Rc_a^{1/4}$$

$k_{eff} = 0.386(0.1735)(765.22 /0.861+765.22)^{1/4} *(77071)^{1/4}$

$k_{eff} = 1.115$ W/m.K

$$q^- = \frac{2\pi.k_{eff}}{\ln(r_o / r_i)}(T_n - T_w)$$

$q^- = 2*\pi*(1.115)*(345\text{-}300)/(\ln(0.0255/0.00635))$

$q^- = 226.65$ W/m

REFERENCES

[1]   A. Fernández-García, E. Zarza, L. Valenzuela, and M. Pérez, "Parabolic-trough solar collectors and their applications," *Renewable and Sustainable Energy Reviews,* vol. 14, pp. 1695-1721, 2010.

[2]   K. Nithyanandam and R. Pitchumani, "Optimization of an encapsulated phase change material thermal energy storage system," *Solar Energy,* vol. 107, pp. 770-788, 2014.

[3]   E. Bellos, C. Tzivanidis, A. Delis, and K. Antonopoulos, "Comparison of a solar driven heat pump heating system with other typical heating systems with TRNSYS," in *Proceedings of the 28th International Conference on Efficiency, Cost, Optimization, Simulation and Environmental Impact of Energy Systems, 30th June–3rd July*, 2015, pp. 176-186.

[4]   N. Aste, M. Beccali, and L. Tagliabue, "Nomograph for rapid technical and economic assessment of solar thermal systems for DHW production," *Solar energy,* vol. 86, pp. 2472-2485, 2012.

[5]   S. Kalogirou, "The potential of solar industrial process heat applications," *Applied Energy,* vol. 76, pp. 337-361, 2003.

[6]   G. Pei, J. Li, and J. Ji, "Analysis of low temperature solar thermal electric generation using regenerative Organic Rankine Cycle," *Applied Thermal Engineering,* vol. 30, pp. 998-1004, 2010.

[7]   W. Duangthongsuk and S. Wongwises, "An experimental study on the heat transfer performance and pressure drop of TiO 2-water nanofluids flowing under a turbulent flow regime," *International Journal of Heat and Mass Transfer,* vol. 53, pp. 334-344, 2010.

[8]   A. S. Ahuja, "Augmentation of heat transport in laminar flow of polystyrene suspensions. I. Experiments and results," *Journal of Applied Physics,* vol. 46, pp. 3408-3416, 1975.

[9]   E. Bellos, C. Tzivanidis, K. Antonopoulos, and G. Gkinis, "Thermal enhancement of solar parabolic trough collectors by using nanofluids and converging-diverging absorber tube," *Renewable Energy,* vol. 94, pp. 213-222, 2016.

[10]   O. García-Valladares and N. Velázquez, "Numerical simulation of parabolic trough solar collector: Improvement using counter flow concentric circular heat exchangers," *International Journal of Heat and Mass Transfer,* vol. 52, pp. 597-609, 2009.

[11]   M. Öztürk, N. Ç. Bezir, and N. Özek, "Optical, energetic and exergetic analyses of parabolic trough collectors," *Chinese Physics Letters,* vol. 24, p. 1787, 2007.

[12]   Z. Zheng, Y. Xu, and Y. He, "Thermal analysis of a solar parabolic trough receiver tube with porous insert optimized by coupling genetic algorithm and CFD," *Science China Technological Sciences,* vol. 59, pp. 1475-1485, 2016.

[13]   S. A. Kalogirou, "A detailed thermal model of a parabolic trough collector receiver," *Energy,* vol. 48, pp. 298-306, 2012.

[14]   C. Tzivanidis, E. Bellos, D. Korres, K. Antonopoulos, and G. Mitsopoulos, "Thermal and optical efficiency investigation of a parabolic trough collector," *Case Studies in Thermal Engineering,* vol. 6, pp. 226-237, 2015.

[15]   R. V. Padilla, G. Demirkaya, D. Y. Goswami, E. Stefanakos, and M. M. Rahman, "Heat transfer analysis of parabolic trough solar receiver," *Applied Energy,* vol. 88, pp. 5097-5110, 2011.

[16]   S. E. Ghasemi, A. A. Ranjbar, and A. Ramiar, "Three-dimensional numerical analysis of heat transfer characteristics of solar parabolic collector with two segmental rings," *J Math Comput Sci,* vol. 7, pp. 89-100, 2013.

[17]   H. Al-Ansary and O. Zeitoun, "Numerical study of conduction and convection heat losses from a half-insulated air-filled annulus of the receiver of a parabolic trough collector," *Solar Energy,* vol. 85, pp. 3036-3045, 2011.

[18]   Y.-L. He, J. Xiao, Z.-D. Cheng, and Y.-B. Tao, "A MCRT and FVM coupled simulation method for energy conversion process in parabolic trough solar collector," *Renewable Energy,* vol. 36, pp. 976-985, 2011.

[19]   A. Mwesigye, W. G. Le Roux, T. Bello-Ochende, and J. P. Meyer, "Thermal and thermodynamic analysis of a parabolic trough receiver at different concentration ratios and rim angles," 2014.

[20]   P. Keblinski, J. A. Eastman, and D. G. Cahill, "Nanofluids for thermal transport," *Materials today,* vol. 8, pp. 36-44, 2005.

[21]   M.-S. Liu, M. C.-C. Lin, I.-T. Huang, and C.-C. Wang, "Enhancement of thermal conductivity with carbon nanotube for nanofluids," *International communications in heat and mass transfer,* vol. 32, pp. 1202-1210, 2005.

[22]   W. Yu, H. Xie, X. Wang, and X. Wang, "Significant thermal conductivity enhancement for nanofluids containing graphene nanosheets," *Physics Letters A,* vol. 375, pp. 1323-1328, 2011.

[23]   S. Murshed, K. Leong, and C. Yang, "Enhanced thermal conductivity of TiO_2—water based nanofluids," *International Journal of Thermal Sciences,* vol. 44, pp. 367-373, 2005.

[24]   M. Kole and T. Dey, "Effect of aggregation on the viscosity of copper oxide–gear oil nanofluids," *International Journal of Thermal Sciences,* vol. 50, pp. 1741-1747, 2011.

[25]   A. Arefmanesh and M. Mahmoodi, "Effects of uncertainties of viscosity models for Al_2O_3–water nanofluid on mixed convection numerical simulations," *International journal of Thermal sciences,* vol. 50, pp. 1706-1719, 2011.

[26]   M. B. Moghaddam, E. K. Goharshadi, M. H. Entezari, and P. Nancarrow, "Preparation, characterization, and rheological properties of graphene–glycerol nanofluids," *Chemical engineering journal,* vol. 231, pp. 365-372, 2013.

[27]   B. C. Pak and Y. I. Cho, "Hydrodynamic and heat transfer study of dispersed fluids with submicron metallic oxide particles," *Experimental Heat Transfer an International Journal,* vol. 11, pp. 151-170, 1998.

[28]   Y. Xuan and W. Roetzel, "Conceptions for heat transfer correlation of nanofluids," *International Journal of heat and Mass transfer,* vol. 43, pp. 3701-3707, 2000.

[29] H. Tiznobaik and D. Shin, "Enhanced specific heat capacity of high-temperature molten salt-based nanofluids," *International Journal of Heat and Mass Transfer,* vol. 57, pp. 542-548, 2013.

[30] F. Yang, X. Qiu, Y. Li, Y. Yin, and Q. Fan, "Specific heat of super carbon nanotube and its chirality independence," *Physics Letters A,* vol. 372, pp. 6960-6964, 2008.

[31] E. De Robertis, E. Cosme, R. Neves, A. Y. Kuznetsov, A. Campos, S. Landi*, et al.*, "Application of the modulated temperature differential scanning calorimetry technique for the determination of the specific heat of copper nanofluids," *Applied Thermal Engineering,* vol. 41, pp. 10-17, 2012.

[32] M. Pastoriza-Gallego, C. Casanova, R. Páramo, B. Barbés, J. Legido, and M. Piñeiro, "A study on stability and thermophysical properties (density and viscosity) of Al 2 O 3 in water nanofluid," *Journal of Applied Physics,* vol. 106, p. 064301, 2009.

[33] V. Singh, S. Sharma, and D. D. Gangacharyulu, "Variation of CuO distilled water based nanofluid properties through Circular Pipe," *Volume,* vol. 3, pp. 414-420.

[34] T.-P. Teng and Y.-H. Hung, "Estimation and experimental study of the density and specific heat for alumina nanofluid," *Journal of Experimental Nanoscience,* vol. 9, pp. 707-718, 2014.

[35] K. Sunil, L. Kundan, and S. Sumeet, "Performance evaluation of a nanofluid based parabolic solar collector—An experimental study," *International Journal of Mechanical and Production Engineering Research and Development (IJMPERD),* vol. 10, pp. 2320-2400, 2014.

[36] N. Basbous, M. Taqi, and N. Belouaggadia, "Numerical Study of a Parabolic Trough Collector Using a Nanofluid," *Asian Journal of Current Engineering and Maths,* vol. 4, pp. 40-44, 2015.

[37] K. Ajay and K. Lal, "An Experimental and CFD Analysis of CuO-H2O (DI) Nanofluid Based Parabolic Solar Collector."

[38] A. Mwesigye, Z. Huan, and J. P. Meyer, "Thermal performance and entropy generation analysis of a high concentration ratio parabolic trough solar collector with Cu-Therminol® VP-1 nanofluid," *Energy Conversion and Management,* vol. 120, pp. 449-465, 2016.

[39] E. Kaloudis, E. Papanicolaou, and V. Belessiotis, "Numerical simulations of a parabolic trough solar collector with nanofluid using a two-phase model," *Renewable Energy,* vol. 97, pp. 218-229, 2016.

[40] B. Kristiawan, E. P. Budiana, and E. R. Dyartanti, "Utilization of Nanofluids Potency as Advanced Htfs on Solar Parabolic Trough Collector Evacuated Tube Receiver," 2013.

[41] S. Ladjevardi, A. Asnaghi, P. Izadkhast, and A. Kashani, "Applicability of graphite nanofluids in direct solar energy absorption," *Solar Energy,* vol. 94, pp. 327-334, 2013.

[42] A. Menbari, A. A. Alemrajabi, and A. Rezaei, "Experimental investigation of thermal performance for direct absorption solar parabolic trough collector (DASPTC) based on binary nanofluids," *Experimental Thermal and Fluid Science,* vol. 80, pp. 218-227, 2017.

[43]	G. Xu, W. Chen, S. Deng, X. Zhang, and S. Zhao, "Performance evaluation of a nanofluid-based direct absorption solar collector with parabolic trough concentrator," *Nanomaterials,* vol. 5, pp. 2131-2147, 2015.

[44]	V. Khullar, H. Tyagi, P. E. Phelan, T. P. Otanicar, H. Singh, and R. A. Taylor, "Solar energy harvesting using nanofluids-based concentrating solar collector," *Journal of Nanotechnology in Engineering and Medicine,* vol. 3, p. 031003, 2012.

[45]	W. Chen, G. Xu, S. Zhao, and X. Zhang, "Numerical Simulation on the Performance of Nanofluid-Based Direct Absorption Solar Collector With Parabolic Trough Concentrator," in *ASME 2016 5th International Conference on Micro/Nanoscale Heat and Mass Transfer*, 2016, pp. V001T05A012-V001T05A012.

[46]	L. M. Jiji and L. M. Jiji, *Heat convection*: Springer, 2006.

[47]	A. Fluent, "Ansys fluent theory guide," *ANSYS Inc., USA,* vol. 15317, pp. 724-746, 2011.

[48]	P. Daniel, Y. Joshi, and A. K. Das, "Numerical investigation of parabolic trough receiver performance with outer vacuum shell," *Solar Energy,* vol. 85, pp. 1910-1914, 2011.

[49]	J. A. Duffie and W. A. Beckman, *Solar engineering of thermal processes*: John Wiley & Sons, 2013.

[50]	R. Schmidt, G. Klingenberg, and M. Woydt, "New lubrication concepts for environmental friendly machines," 2006.

[51]	J. C. Maxwell, *A treatise on electricity and magnetism* vol. 1: Clarendon press, 1881.

[52]	A. Einstein, "Eine neue bestimmung der moleküldimensionen," *Annalen der Physik,* vol. 324, pp. 289-306, 1906.

[53]	T. Sokhansefat, A. Kasaeian, and F. Kowsary, "Heat transfer enhancement in parabolic trough collector tube using Al 2 O 3/synthetic oil nanofluid," *Renewable and Sustainable Energy Reviews,* vol. 33, pp. 636-644, 2014.

[54]	S. Senthilraja, K. Vijayakumar, and R. Gangadevi, "A comparative study on thermal conductivity of Al2O3/water, CuO/water and Al2O3–CuO/water nanofluids," *Digest Journal of Nanomaterials and Biostructures,* vol. 10, pp. 1449-1458, 2015.

[55]	T. Tayebi, A. J. Chamkha, M. Djezzar, and A. Bouzerzour, "Natural Convective Nanofluid Flow in an Annular Space Between Confocal Elliptic Cylinders," *Journal of Thermal Science and Engineering Applications,* vol. 9, p. 011010, 2017.

[56]	A. C. Yunus, "Heat transfer: a practical approach," *MacGraw Hill, New York,* 2003.

[57]	Company of Greenhill EnviroTechnologies Inc. (2016, 04 May). *Okapi Solar Calculator App*. Available: http://www.greenhillenvirotechnologies.com/android-and-java-apps/okapi-solar-app-for-android

[58]	A. F. Handbook, "American society of heating, refrigerating and air-conditioning engineers," *Inc.: Atlanta, GA, USA,* 2009.